

THESIS FOR THE DEGREE OF LICENTIATE OF ENGINEERING

# Molecular Astrophysics in Star-forming Regions with the Odin Satellite

CARINA M. PERSSON



**CHALMERS**

Department of Radio and Space Science  
CHALMERS UNIVERSITY OF TECHNOLOGY  
Göteborg, Sweden 2006

# **Molecular Astrophysics in Star-forming Regions with the Odin Satellite**

CARINA M. PERSSON

© Carina M. Persson, 2006

ISSN 1652 – 9103

Technical Report No. 2006:17L

Radio Astronomy & Astrophysics Group

Department of Radio and Space Science

Chalmers University of Technology

SE-412 96 Göteborg, Sweden

Phone: +46 (0)31-772 1000

## **Contact information:**

Carina M. Persson

Onsala Space Observatory

Chalmers University of Technology

SE-439 92 Onsala, Sweden

Phone: +46 (0)31-772 5537

Fax: +46 (0)31-772 5590

Email: [carina.persson@chalmers.se](mailto:carina.persson@chalmers.se)

*Cover: An illustration of the Odin satellite, and part of a spectral scan towards the Orion KL region with the Odin satellite.*

Printed by Chalmers Reproservice  
Chalmers University of Technology  
Göteborg, Sweden 2006

# Molecular Astrophysics in Star-forming Regions with the Odin Satellite

CARINA M. PERSSON

Department of Radio and Space Science  
Chalmers University of Technology

## Abstract

The interstellar medium is the cradle of life, stars and planets in the evolving Universe. Stars are born deep inside cold and dark molecular clouds, and affect the dynamical conditions in local regions by powerful winds, outflows, and by supernova explosions. Optical light from star-formation is trapped within the clouds because of absorption by dust grains. However, radiation is able to escape through the gas and dust in the infrared and radio spectral regions. In addition, the chemical evolution of molecules is very sensitive to temperature, density and radiation field. Thus, radio and submm observations of molecules are an excellent probe of both the physical and chemical conditions in star-forming regions and the interstellar medium in general.

Some important molecules are difficult to observe with ground-based telescopes due to the Earth's obscuring atmosphere. Hence observations from space are necessary in these spectral regions. The launch of the Odin<sup>1</sup> satellite in 2001, enabled observations of molecular oxygen and the ground-state water transition that traces shocks and star-formation.

One of the big unanswered questions in astronomy is the origin of structure. During the cosmic Dark Ages after the Big Bang, the Universe evolved from uniformity to the structures of galaxies, clusters, and voids that we observe today. Direct observations from the Dark Ages are most commonly believed to be impossible. But our aim in the search for the Primordial molecules is exactly this – to perform observations of resonant spectral lines from the cosmic Dark Ages.

To study the conditions in a star-forming region, including an unbiased search for new molecules, a spectral line survey has been performed toward the Orion KL massive star-forming region. We have observed 347 spectral lines from 38 molecules including isotopologues, while 19% of the lines remain unidentified. Six water lines are detected including the water isotopologues H<sub>2</sub><sup>17</sup>O, H<sub>2</sub><sup>18</sup>O and HDO. The total emission is dominated by CO, H<sub>2</sub>O, SO<sub>2</sub>, SO, <sup>13</sup>CO and CH<sub>3</sub>OH. Species with the largest number of lines are CH<sub>3</sub>OH, (CH<sub>3</sub>)<sub>2</sub>O, SO<sub>2</sub>, <sup>13</sup>CH<sub>3</sub>OH, CH<sub>3</sub>CN and NO.

**Keywords:** ISM: abundances – ISM: molecules – Astrobiology – Molecular data – ISM: individual objects: Orion KL – Radio lines: ISM – Submillimeter – line: formation – line: identification

---

<sup>1</sup>Odin is a Swedish-led satellite project funded jointly by the Swedish National Space Board (SNSB), the Canadian Space Agency (CSA), the National Technology Agency of Finland (Tekes) and Centre National d'études Spatiales (CNES). The Swedish Space Corporation was the prime contractor and also is responsible for the satellite operation.



## Research contributions

This thesis is based on the work reported in

- **Paper I:** A.O. Henrik Olofsson, Carina M. Persson, N. Koning, T.I. Hasegawa, P. Bergman, P. Bernath, J. Black, U. Frisk, W. Geppert, Å. Hjalmarson, S. Kwok, B. Larsson, A. Lecacheux, A. Nummelin, M. Olberg, Aa. Sandqvist, and E.S. Wirström: *A spectral line survey of Orion KL from 486-492 and 541-577 GHz with the Odin satellite. I. The Data*  
To be submitted to Astronomy & Astrophysics
  - **Paper II:** Carina M. Persson A.O. Henrik Olofsson, N. Koning, T.I. Hasegawa, P. Bergman, P. Bernath, J. Black, U. Frisk, W. Geppert, Å. Hjalmarson, S. Kwok, B. Larsson, A. Lecacheux, A. Nummelin, M. Olberg, Aa. Sandqvist, and E.S. Wirström: *A spectral line survey of Orion KL from 486-492 and 541-577 GHz with the Odin satellite. II. Data analysis*  
To be submitted to Astronomy & Astrophysics
- and
- *Searches for Primordial molecules from the Early Universe:*  
Carina M. Persson, P. Encrenaz, Å. Hjalmarson, M. Olberg, and G. Rydbeck.  
**Chapter 3** and:  
Encrenaz, P., Persson, C.M., Hjalmarson, Å, de Bernardis, P., Chabaud, G., Daniel, J.Y., Frisk, U., Maoli, R., Masi, S., Melchiorri, B., Melchiorri, F., Olberg, M., Pagani, L., Rosmus, P., Rydbeck, G., Sandqvist, Aa., and Signore, M.  
*Progress in searches for primordial resonant lines using the Odin satellite*  
IAUS, 231, 241 (2005)



## Acknowledgements

There are a few people that I want to mention especially. First of all — I am very grateful to my supervisor Michael Olberg who has been the very best supervisor for me. And many thanks to my assistant supervisor Åke Hjalmarson whose encouragement is very appreciated, to John Black for his kindness and knowledge, and to Per Bergman, Gustaf Rydbeck, and Roger Hammargren who always are very helpful. And what would I have done without my special friend Eva, and Henrik, Paula, Susanne, Julia, Vivi, Margareta, Ingrid, Cathy, Monica, Eva N, Eva A, Camilla, Raquel, and all colleagues and staff members at Onsala and the whole Astronomy and Astrophysics group. Thanks also to the former head of the observatory Roy Booth, to the new, Hans Olofsson, and to Pierre Encrenaz from Observatoire de Paris.

To all my friends and teachers at the University of Uppsala, Leif Karlsson at the Physics department, and especially the Astronomy department and the Galaxy group including Nils Bergvall, Erik Zackrisson, and Kjell Olofsson, as well as Kjell Eriksson and Bengt Edvardsson – thanks a lot for your encouragement. And also many thanks to Johannes Ortner, director for the Alpbach Summer School, Austria.

And to my family – my wonderful, lovely, best of all children! Andreas, Anna, Maria, och Rebecca. Tack för att ni alltid är de bästa barnen som finns! Och tack! mamma och pappa och min moster Anita för all hjälp. And to Felicia, and to you Kaj, who have my heart.

I am grateful to the Swedish National Space Board (SNSB) for support of this PhD project.

Carina

I also participated as a co-investigator in the following papers

- Wirström, E.S., Bergman, P., Olofsson, A.O.H., Frisk, U., Hjalmarson, Å., Olberg, M., Persson, C.M., and Sandqvist, Aa.,  
*Odin CO and  $^{13}\text{CO}$   $J=5-4$  mapping of Orion KL – a step towards accurate water abundances*  
Astronomy & Astrophysics, 453, 979 (2006)
- Wilson, C.D., Booth, R.S., Olofsson, A.O.H., Olberg, M., Persson, C.M., Sandqvist, Aa., Buat, V., Encrenaz, P.J., Fich, M., Frisk, U, Gerin, M., Johansson, L.E.B., Rydbeck, G., and Wiklind, T.  
*Upper limits to the water abundance in starburst galaxies*  
Submitted to Astronomy & Astrophysics
- Berciano Alba, A., Borges da Silva, P., Eichelberger, H, Giovacchini, F, Godolt, M., Hasinger, G., Lerchster, M., Lusset, V., Mattana, F., Mellier, Y., Michalowski, M., Monteserin-Sanches, C., Noviello, F., Persson, C.M., Santovincenzo, A., Schneider, P., Zhang, M., and Östman, L.  
*DEMON: a Proposal for a Satellite-Borne Experiment to study Dark Matter and Dark Energy*  
astro-ph/0606010  
Accepted for publication in the SPIE conference proceedings (2006):  
Space Telescopes and Instrumentation II: Ultraviolet to Gamma Ray (AS02)  
Part of SPIE's International Symposium on Astronomical Telescopes and Instrumentation

# Contents

Abstract . . . . .	i
Research contributions . . . . .	iii
Acknowledgements . . . . .	5
<b>1 The Interstellar Medium</b>	<b>1</b>
1.1 Introduction . . . . .	1
1.2 Dust grains and ices . . . . .	2
1.3 Astrochemistry . . . . .	4
1.3.1 Water . . . . .	8
1.4 Molecular environments . . . . .	10
1.4.1 HII regions . . . . .	11
1.4.2 Photodissociation or Photon Dominated Regions . . . . .	11
1.4.3 Hot cores . . . . .	12
1.4.4 Shocks and outflows . . . . .	13
1.4.5 Cold dark clouds . . . . .	13
1.4.6 Giant Molecular Clouds (GMCs) . . . . .	13
<b>2 Star-formation</b>	<b>15</b>
2.1 Jeans mass and star-formation . . . . .	15
2.2 Heating and cooling . . . . .	16
2.3 The first stars . . . . .	18
<b>3 Searches for Primordial Molecules in the Early Universe</b>	<b>19</b>
3.1 The beginning . . . . .	19
3.2 Elements of our primordial medium . . . . .	21
3.3 Resonant scattering . . . . .	23
3.4 Implications . . . . .	25
3.5 Observations . . . . .	25
3.5.1 Previous observations . . . . .	25
3.5.2 Our Odin observations . . . . .	26
3.6 Future prospects . . . . .	28

<b>4 Introduction to Paper I and Paper II</b>	<b>29</b>
4.1 The Odin satellite . . . . .	29
4.2 The Orion nebula . . . . .	30
4.3 Summary of Paper I and Paper II . . . . .	33
<b>Paper I</b>	<b>37</b>
<b>Paper II</b>	<b>61</b>
<b>Abstract of poster</b>	<b>109</b>
<b>A Tools of astronomy</b>	<b>113</b>
A.1 Radiative transfer . . . . .	113
A.1.1 Optical depth and source function . . . . .	114
A.1.2 Solution of the transport equation . . . . .	115
A.1.3 Special cases . . . . .	116
A.1.4 Discrete processes – spectral line theory . . . . .	118
A.1.5 Photon creation, destruction, scattering and conversion . . . . .	120
A.1.6 Types of equilibrium . . . . .	121
A.1.7 Critical density . . . . .	122
A.2 Radioastronomy . . . . .	123
A.3 Column densities . . . . .	124
A.3.1 Rotational diagram . . . . .	125
<b>Bibliography</b>	<b>127</b>

# Chapter 1

## The Interstellar Medium

### 1.1 Introduction

A galaxy consist of billions of stars, and in between there is an important constituent of gas and dust particles called the Interstellar Medium (ISM). Of all visible matter in our Galaxy approximately 15% is composed of interstellar gas and dust. We observe this very dilute gas by its own emission and by the absorption of starlight that travels trough it.

The ISM might at first glance seem uninteresting, but there are a number of reasons to study it. First, it all starts here. The Universe is continuously evolving, and the stars are born deep within cold molecular clouds. By studying the ISM we gain information about the necessary conditions for star-formation.

When the stars end their lives (in different ways depending on their initial mass) they return most of the gas to the ISM. Gas is also lost by the stars during their entire lifetimes in stellar winds. Almost everything in the Universe is thus recycled. But when the gas is returned to the ISM, the composition is not the same anymore. After the Big Bang the primordial composition of the ISM was about (by mass) 75% of hydrogen and 25% of helium. Today most of the ISM still has approximately this composition, but now there are other heavier elements as well, especially in the dust. The elements have been processed within the hot cores of stars in different nucleosynthesis processes, where the hydrogen nuclei are combined into helium in the proton-proton chain or CNO-cycle, helium nuclei combine into carbon or oxygen in the triple alpha process, etc. Elements heavier than iron can only be produced when very massive stars explode as supernovas. Thus, early generation stars contained (almost) only hydrogen and helium, while the next generation of stars, and their possible solar systems, contained all other elements produced by the previous stars. So by studying the relative elemental abundances of the ISM, we can obtain information about the chemical evolution in our Galaxy, and the history of star-formation including different types of supernovae.

The ISM is also a unique chemical laboratory characterised by very low densities and temperatures (typically a few tens of Kelvins) not available on Earth, allowing studies of chemistry otherwise not accessible. For instance the radical  $\text{HCO}^+$  was first observed in the ISM and only later observed and confirmed in the laboratory (summary is given in Rydbeck & Hjalmarson 1985).

Another example of the importance of studies of the ISM is deuterium observations. Since no efficient processes of deuterium (isotope of hydrogen) production are known, almost all existing deuterium today is a relic from the Big Bang. If we measure the primordial abundance of deuterium in the local or extra-galactic ISM, a limit on the primordial value of the relative abundance of  $[\text{D}/\text{H}]$  can be obtained. This value is used to calculate the baryonic density in the Universe, thus constraining the Big Bang Nucleosynthesis.

The ISM is not a homogeneous gas cloud with equal density and temperature spread evenly throughout the Galaxy. Our Galaxy, the Milky Way, contains  $\sim 4\text{--}8 \times 10^9 M_\odot$  of neutral hydrogen, and about half of that amount exist as molecular hydrogen. Almost all of the molecular gas is piled up in a ring 4 kpc from the centre of the Milky Way. The neutral gas is found across the whole Galaxy. The sizes of the clouds range from 0.1 pc for dark, isolated cloudlets to more than 10 pc for Giant Molecular Cloud complexes. The density is typically higher in the spiral arms and towards the centre, and can vary by many orders of magnitude – from less than 1 particle per  $\text{cm}^{-3}$  to  $10^7 \text{ cm}^{-3}$  in dense clouds – while the temperature variation is smaller (from tens of K to millions of K). To get a feeling for what a dense medium in space means we can compare this with the best vacuum on Earth, which has a density of  $10^6 \text{ cm}^{-3}$ , or the air at sea level with a density of  $3 \times 10^{19} \text{ cm}^{-3}$ .

On small scales ( $\lesssim 1$  kpc) the ISM forms a multi-phase medium with different co-existing phases. Low density gas with high temperature is in pressure equilibrium with higher density, lower temperature gas. A warm, diffuse medium with a temperature of about 8000 K corresponds to a density of  $\sim 0.1 \text{ cm}^{-3}$ , while colder gas of 100 K corresponds to a density of  $10 \text{ cm}^{-3}$ . The even denser molecular clouds are gravitationally bound entities. A hot plasma phase also exists with a temperature of  $10^6$  K, and a number density of  $10^{-3} \text{ cm}^{-3}$ . Most of the mass is in the dense phase, but the diffuse plasma occupies most of the volume. The gas material passes continuously between the different phases.

## 1.2 Dust grains and ices

In addition to the gas the ISM contains approximately  $\sim 1\%$  (by mass) of small dust particles ( $0.01 \mu\text{m}$ – $1 \mu\text{m}$ ) consisting of solid state molecules heavier than hydrogen, such as silicates, graphite, amorphous carbon (soot), and polycyclic aromatic hydrocarbons (PAHs). The bulk of the dust grains originates in oxygen-

rich M giants (silicate dust), radio-luminous OH/IR stars, super-giants, and carbon stars (sooty particles). They form near the photosphere of the star together with molecules and radiation pressure on the grains drives the circumstellar wind, which injects the dust and gas into the ambient ISM. Supernova shock waves distribute the dust over large scales, and the dust is subsequently mixed into the ISM.

Dust particles can absorb and scatter photons, and this shields the interior parts of a cloud enabling molecules to survive. The absorption of radiation heats the grains to radiate in infrared, i.e. they can absorb uv- and visible light and transform the radiation to longer wavelengths. The absorption of UV photons also causes electrons to be ejected from the grains, which is an important heating source of the gas.

Many gas-phase reactions demand a "starter" molecule. This can be provided by molecular formation *on the surface of dust grains*, where a complicated chemistry is occurring including (almost) all of the H<sub>2</sub> production. The formation rate primarily depends on the nature of the grain surface, which creates an environment to prolong the collision time of the elements, and hence the probability for a reaction to occur increases. At 10 K the H, D, C, O and N atoms have sufficient mobility to scan the grain surface to find a reaction partner.

In colder regions the surface is often covered with a layer of volatile material. This is typically ices of H<sub>2</sub>O, CH<sub>3</sub>OH, CO<sub>2</sub>, CO, CH<sub>4</sub>, NH<sub>3</sub>, and OCS. H<sub>2</sub>O is the dominant species and CO<sub>2</sub> is the second most common with about 20 percent of the water abundance. However, in the gas-phase CO<sub>2</sub> is surprisingly rare. The dust particles can acquire these icy grain mantles through the slow, but efficient, accretion of species in the gas-phase. The sticking coefficients are expected to be close to unity for heavy species at low temperatures. The time for removal from the gas-phase to the dust is about  $3 \times 10^9 / n_H$  years, where  $n_H$  is the hydrogen nucleon number density. With a density of  $10^4 \text{ cm}^{-3}$ , the depletion time scale is only about  $3 \times 10^5$  years, which is less than the expected lifetime of dense cores in GMCs (see section 1.4.6). Icy grain mantles have been observed with SWS (Short Wavelength Spectrometer) on-board the ISO-satellite between 2.5 and 200  $\mu\text{m}$  (Gibb et al. 2004).

In the *amorphous ice* on the grain surfaces a complex chemistry is taking place. On Earth atoms and organisms demand liquid water to be able to form larger species. But at the cold temperatures present in space, the water will be in the form of ice. The water molecules are then ordered in a rigid crystalline structure and this recoils other species. However, in vacuum, cold water molecules behave differently and produce an amorphous ice, which has similar properties to liquid water. The hydrogen bonds between the water molecules redistribute constantly and rapidly, and this creates an excellent environment for molecules to form. As much as 10 percent of the water volume can consist of other species.

The molecules get off the dust grains by different methods: sputtering in

shocks, X-ray or UV-radiation, thermal desorption, cosmic rays, or chemical energy of reactions ( $\text{H}_2$ ).

### 1.3 Astrochemistry

In radio and sub-mm astronomy we mainly observe the low-energy rotational molecular transitions from molecular clouds that are too cold to radiate in the infrared or visible regions of the spectrum. Molecules influence the birth and distribution of stars and structure of galaxies, and the entire cosmos is on the large scale chemically controlled. Radio astronomy and the study of molecules are therefore important parts of astronomy in general. Molecular astrophysics began with the discovery of CH,  $\text{CH}^+$ , and CN in the late 1930s. The first observation demonstrating the existence of dense star-forming gas was the detection of the ammonia  $J = 1, K = 1$  inversion line in 1968 (Cheung, Rank and Townes) towards the Galactic Centre. The observed lines also made a temperature estimation possible, and also showed that polyatomic interstellar molecules did exist.

Astrochemistry is the study of interstellar molecules, their formation routes and the use of these species to gain information about the ISM. Since the space offers low density and temperature, highly reactive, chemically unstable species on Earth can therefore be quite abundant in certain regions. These include ions like  $\text{HCO}^+$ , and radicals like OH, CH and CN, which are electrons with unpaired electrons. But the overwhelmingly most abundant molecule in the ISM is  $\text{H}_2$  (99.99% of all molecules). As a consequence of no allowed dipole transitions in the symmetric  $\text{H}_2$ , most of the contents in cold molecular clouds is thus invisible. Molecular hydrogen can only be seen in infrared, through vibrational-rotational transitions, in most cases tracing the hot gas. To be able to trace the cold  $\text{H}_2$  gas, the second most common molecule CO, with an abundance relative to  $\text{H}_2$  of  $\sim 10^{-4}$ , is used assuming co-spatial existence. CO is easily excited at modest densities and temperatures and is very tightly bound. HI is observed in the hyperfine transition at 21 cm (1420 MHz), which is a low-probability transition in the ground energy level, when the electron changes its spin relative to the proton. Other detected molecules are very familiar to us like water, ammonia and formaldehyde.

Around 150 molecules have been detected in space as seen in Table 1.1. Compounds of the elements with the highest abundances, hydrogen, carbon, oxygen, and nitrogen, constitute the major part of the detected molecules. Molecules that form from heavier refractory elements, such as S, Si or Mg, often reside in the dust particles. Larger carbon-bearing species like polycyclic aromatic hydrocarbons, PAHs, may also be present in ISM.

Table 1.1: Detected interstellar molecules as of October 2006, (149+). Cyclic form is labelled c-, and linear form with l-. A question mark is added to a not confirmed detection. Credit: Åke Hjalmarson.

Hydrogen compounds				
H <sub>2</sub> <sup>a</sup>	HD <sup>a</sup>	H <sub>3</sub> <sup>+</sup>	H <sub>2</sub> D <sup>+</sup>	O <sub>2</sub>
Hydrogen and Carbon compounds				
CH <sup>b</sup>	CH <sup>+</sup> <sup>a</sup>	C <sub>2</sub> <sup>a</sup>	CH <sub>2</sub>	C <sub>2</sub> H
C <sub>3</sub>	CH <sub>3</sub>	C <sub>2</sub> H <sub>2</sub> <sup>d</sup>	l-C <sub>3</sub> H	c-C <sub>3</sub> H
CH <sub>4</sub> <sup>d</sup>	C <sub>4</sub>	c-C <sub>3</sub> H <sub>2</sub>	l-H <sub>2</sub> CCC	C <sub>4</sub> H
C <sub>5</sub> <sup>c</sup>	C <sub>2</sub> H <sub>4</sub> <sup>c</sup>	C <sub>5</sub> H	l-H <sub>2</sub> C <sub>4</sub>	HC <sub>4</sub> H <sup>c</sup>
CH <sub>3</sub> C <sub>2</sub> H	C <sub>6</sub> H	HC <sub>6</sub> H <sup>c</sup>	H <sub>2</sub> C <sub>6</sub>	C <sub>7</sub> H <sup>c</sup>
CH <sub>3</sub> C <sub>4</sub> H	CH <sub>3</sub> C <sub>6</sub> H	C <sub>8</sub> H	C <sub>6</sub> H <sub>6</sub> <sup>c</sup>	
Hydrogen, Oxygen and Carbon compounds				
OH <sup>b,d</sup>	CO <sup>b,d</sup>	CO <sup>+</sup> <sup>d</sup>	H <sub>2</sub> O <sup>d</sup>	HCO
HCO <sup>+</sup> <sup>d</sup>	HOC <sup>+</sup>	C <sub>2</sub> O	CO <sub>2</sub> <sup>d</sup>	H <sub>3</sub> O <sup>+</sup> <sup>d</sup>
HOCO <sup>+</sup>	H <sub>2</sub> CO <sup>d</sup>	C <sub>3</sub> O	CH <sub>2</sub> CO	HCOOH <sup>d</sup>
H <sub>2</sub> COH <sup>+</sup>	CH <sub>3</sub> OH <sup>d</sup>	CH <sub>2</sub> CHO	CH <sub>2</sub> CHCHO	HC <sub>2</sub> CHO
C <sub>5</sub> O	CH <sub>3</sub> CHO	c-C <sub>2</sub> H <sub>4</sub> O	CH <sub>2</sub> CHOH	c-C <sub>3</sub> H <sub>2</sub> O
CH <sub>3</sub> OCHO <sup>d</sup>	CH <sub>3</sub> COOH	CH <sub>2</sub> OHCHO	(CH <sub>3</sub> ) <sub>2</sub> O	CH <sub>3</sub> CH <sub>2</sub> OH
CH <sub>3</sub> CH <sub>2</sub> CHO	(CH <sub>3</sub> ) <sub>2</sub> CO	HOCH <sub>2</sub> CH <sub>2</sub> OH <sup>d</sup>	C <sub>2</sub> H <sub>5</sub> OCH <sub>3</sub>	(CH <sub>2</sub> OH) <sub>2</sub> CO?
Hydrogen, Nitrogen and Carbon compounds				
NH <sup>a,d</sup> (ND?)	CN <sup>b,d</sup>	N <sub>2</sub> <sup>a</sup>	NH <sub>2</sub> <sup>a,d</sup>	HCN <sup>d</sup>
HNC <sup>d</sup>	N <sub>2</sub> H <sup>+</sup>	NH <sub>3</sub> <sup>d</sup>	HCNH <sup>+</sup>	H <sub>2</sub> CN
HCCN	C <sub>3</sub> N	CH <sub>2</sub> CN	CH <sub>2</sub> NH	HC <sub>2</sub> CN <sup>d</sup>
HC <sub>2</sub> NC	NH <sub>2</sub> CN	C <sub>3</sub> NH	CH <sub>3</sub> CN <sup>d</sup>	CH <sub>3</sub> NC
HC <sub>3</sub> NH <sup>+</sup>	HC <sub>4</sub> N <sup>c</sup>	C <sub>5</sub> N	CH <sub>3</sub> NH <sub>2</sub>	CH <sub>2</sub> CHCN
HC <sub>5</sub> N	HC <sub>7</sub> N	HC <sub>9</sub> N	HC <sub>11</sub> N	CH <sub>3</sub> CH <sub>2</sub> CN
CH <sub>3</sub> C <sub>3</sub> N	CH <sub>2</sub> CCHCN	CH <sub>3</sub> C <sub>5</sub> N	c-C <sub>2</sub> H <sub>4</sub> NH?	CH <sub>2</sub> CNH
Hydrogen, Nitrogen, Oxygen and Carbon compounds				
NO	HNO	N <sub>2</sub> O	HNCO <sup>d</sup>	NH <sub>2</sub> CHO <sup>d</sup>
CH <sub>3</sub> CONH <sub>2</sub>	NH <sub>2</sub> CH <sub>2</sub> COOH?			
Other species (containing S, Si, Na, K, Cl, F, Al, Mg, Fe, P)				
SH	CS <sup>d</sup>	SO <sup>d</sup>	SO <sup>+</sup>	NS
SiH	SiC <sup>c</sup>	SiN	SiO	SiS
HCl	NaCl <sup>c</sup>	AlCl <sup>c</sup>	KCl <sup>c</sup>	HF
AlF <sup>c</sup>	CP <sup>c</sup>	PN	H <sub>2</sub> S <sup>d</sup>	C <sub>2</sub> S
SO <sub>2</sub> <sup>d</sup>	OCS <sup>d</sup>	HCS <sup>+</sup>	c-SiC <sub>2</sub>	SiCN <sup>c</sup>
SiNC <sup>c</sup>	NaCN <sup>c</sup>	MgCN <sup>c</sup>	MgNC <sup>c</sup>	AlNC <sup>c</sup>
H <sub>2</sub> CS <sup>d</sup>	HNCS	C <sub>3</sub> S	c-SiC <sub>3</sub>	SiH <sub>4</sub> <sup>c</sup>
SiC <sub>4</sub> <sup>c</sup>	CH <sub>3</sub> SH	C <sub>5</sub> S	FeO	CF <sup>+</sup>
Polycyclic Aromatic Hydrocarbons (PAHs)				

<sup>a</sup> Detected in visible/UV absorption. <sup>b</sup> Detected in visible/UV absorption, and in radio. <sup>c</sup> Only circumstellar species. <sup>d</sup> Also detected in comets.

There are a number of different routes to the production of molecules, where one major formation process occurs on the surface of dust grains. The problem of *gas-phase* reactions is one of energetics. When two atoms collide then cannot form a bound system unless energy can be removed, for instance in a simultaneous collision of a third atom or by emission of a photon during the collision. Otherwise the atoms will merely bounce off each-other. On Earth the density is very high and molecules form easily in three-body collisions. In space the density is too low for this process to occur efficiently, except in the circumstellar envelopes of cold, late-type, post-AGB stars, which offer a warm and dense environment giving a rich chemistry. As seen in Table 1.1 some molecules such as  $C_5$ ,  $C_7H$ , and  $HC_6H$  among others are only detected in these regions.

Since no three-body collisions occur in the ISM, instead efficient *ion-molecule* reactions drive most of the interstellar chemistry, and in high temperature gas it is *neutral-neutral* reactions. The colliding species can be atoms or molecules. The neutral-neutral reactions typically have energy barriers of the order of  $\sim 100$  K, and are only about 1 per cent as likely to occur as are ion-molecule reactions at low temperatures. With increasing temperature the reactions become more efficient. Thus a rich gas-phase chemistry needs warm gas or the presence of ions, which are produced by cosmic rays (relativistic protons or electrons), or UV-radiation from nearby hot, young stars. The most important ion is  $H_3^+$  which starts most other reactions.

Molecules can also be produced by *radiative association*, when the energy sink is a photon. Two atoms collide and form an excited molecule which radiatively decays to the ground state before it dissociates. But the probability is generally very low for these reactions to occur.

Destruction of molecules occurs by different processes, such as *dissociative recombination*. An ambient free electron recombines with a molecular ion and creates an energetic, unstable neutral molecule. The molecule can autoionize again, losing the electron, or fall apart into its neutral species. This reaction increases slowly as the temperature falls. An illuminating case is the reaction  $H_3O^+ + e^-$ , which forms more  $OH + 2H$  than  $H_2O + H$ . Another destruction source is energetic radiation. Molecules do not in general survive if the temperature is about ten times hotter than in the Earth's atmosphere. In dense regions very complex molecules can be produced since the outer layer of the cloud is an effective shield against the UV radiation. But if the clouds are diffuse, the incoming UV photons destroy larger molecules faster than their production, so only small and simple molecules can survive. Some molecules like  $H_2$  and  $CO$  protect themselves with *self-shielding*. This is possible since the destruction process occurs in a number of very narrow spectral bands. The radiation outside these bands does not affect the molecule.  $CO$  is also shielded by  $H_2$ .

Diagnosis of molecular clouds depends on molecular physics. An atom or molecule absorbs and emits radiation at wavelengths that are characteristic of

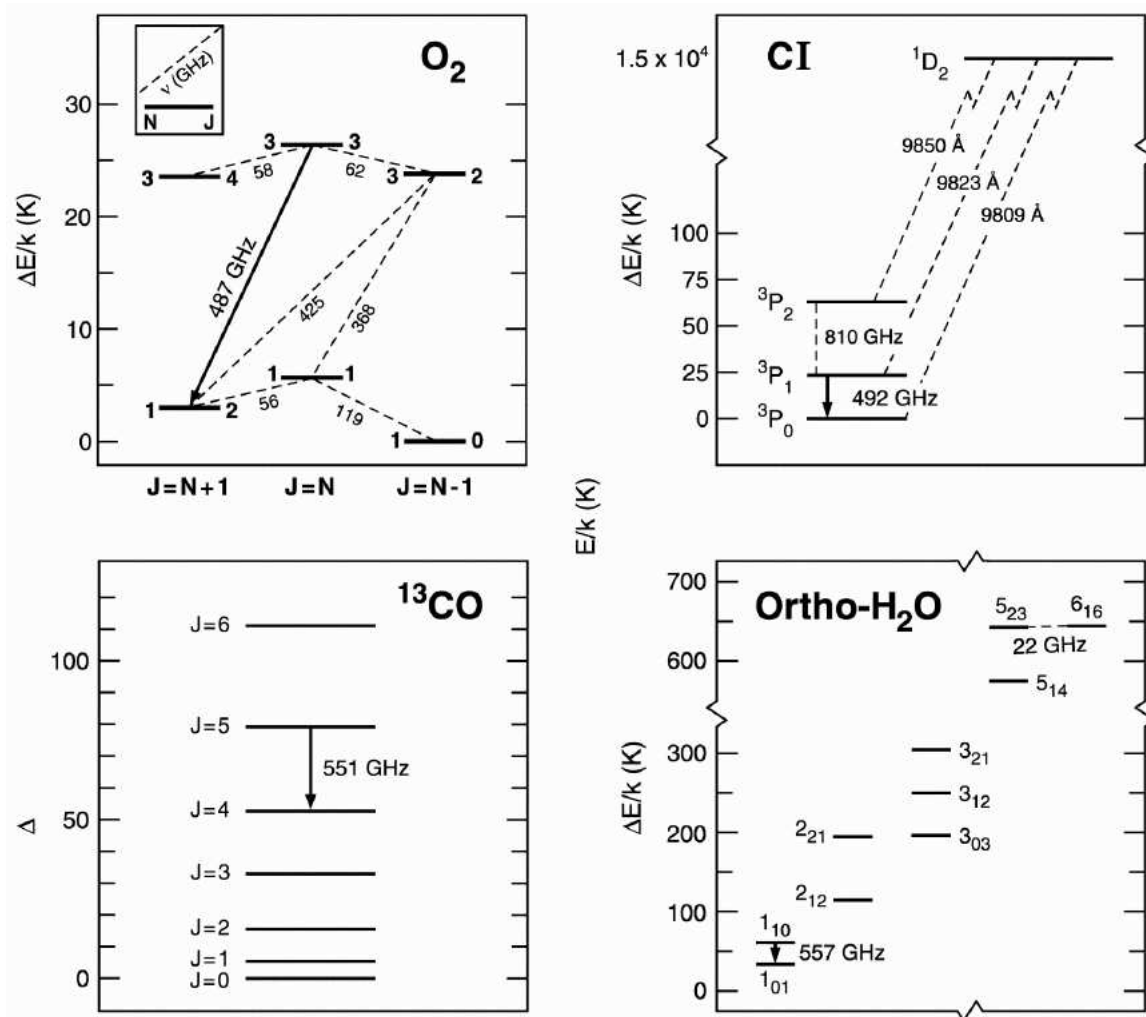


Figure 1.1: Energy level diagrams of O<sub>2</sub>, Cl, <sup>13</sup>CO and *o*-H<sub>2</sub>O. Credit: Gary Melnick.

the species. The energy level diagrams of O<sub>2</sub>, Cl, <sup>13</sup>CO and *o*-H<sub>2</sub>O in Fig. 1.1 show some of the lowest rotational transitions within the first vibrational state for each species. The transitions observed with the SWAS satellite are marked. The Odin satellite observe all these lines, and more. The magnetic dipole transition  $1_1 - 1_0$  of O<sub>2</sub> at 118.750 GHz is Odin's most sensitive search tool. Molecular oxygen has been shown to be orders of magnitude less abundant than expected from chemical models (Pagani et al. 2003), and just has been marginally detected in the dense molecular core  $\rho$  Oph A (Liseau et al. 2005).

An object may appear different in different transitions of the same molecule or in lines of different species. This is a consequence of the response by the molecules to the physical conditions in the medium, including temperature,

abundance, and the background radiation, and this determines the strength of the spectral features of the species. Some molecules have very high critical densities, e.g. CN or CS. Thus these species radiate most strongly when the density is high, and are therefore excellent tracers of high-density gas. Other molecules such as CO have a low critical density and are easily observed from large regions. The excitation temperature can be directly determined by observing an optically thick transition, whereas the column density is derived from optically thin transitions (appendix A).

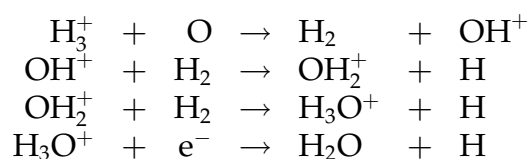
### 1.3.1 Water

The water molecule is of special interest for a number of reasons – first as a key molecule for life as we know it (Brack 2002). The origin of water in the ISM and how it is connected to star-formation is of clear astrobiological interest. Water is also an important ice constituent on the surface of dust grains, and provides an excellent environment to form and shield molecular production. It also helps the coagulation process that produces planets and comets, which are formed by grains, rocky debris, and ices. Like planets, comets must form around other stars than our sun, as in fact suggested by Odin’s detections of H<sub>2</sub>O and NH<sub>3</sub> in the mass-loss winds from the C-rich star IRC+10216 and the O-rich star W Hya (Hasegawa et al. 2006). Their delivery of volatiles to the planets via a heavy bombardment, as in the case of our young Earth, may be important for the formation of oceans and atmospheres and the life itself. In addition, water is vital to the understanding of oxygen chemistry, and also an important cooling agent in warm star-forming regions, where the abundance is relatively high (read more in chapter 2.2).

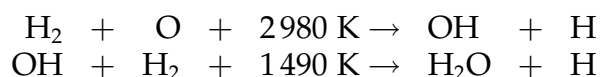
In 1969, Cheung et al. detected water emission for the first time in a high energy maser amplifying transition, towards three sources – the Orion Nebula, Sgr B2 and W49. But due to the Earth’s atmosphere which is completely opaque around the strongest transitions, it is necessary to perform observations from space-borne satellites. The ISO satellite, operational between November 1995 and May 1998, observed water at wavelengths from 2.5 to 240  $\mu\text{m}$  (infrared spectral region) and measured the water abundance both in vapour and solid form (review in Cernicharo & Crovisier 2005). The Spitzer Space Telescope was launched August 2003, on a 2.5-year mission, to obtain images and spectra between wavelengths of 3 and 180  $\mu\text{m}$ . The SWAS satellite, launched in December 1998 and operating during 5.5 years, performed extensive, simultaneous observations of the rotational ground state transition of gas-phase *o*-H<sub>2</sub>O, <sup>13</sup>CO  $J = 5 - 4$ , and CI  $^3P_1 - ^3P_0$  lines in thousands of lines-of-sight. The Odin satellite (see Sect. 4.1), launched a few years later in 2001, was a more sensitive next step after SWAS, and continued the observations of rotational ground state water as well of its important isotopologues.

The results of all these observations indicate that the water abundance relative to molecular hydrogen is low in the gas-phase of dark cold clouds, about  $10^{-8}$ – $10^{-9}$ , where it mostly (98%) resides in the ices on the dust grains. In shocked gas and warm star-forming regions, where water is released from the ices on dust grains and effective chemical reactions produce large amounts of water, high gas-phase abundances of about  $10^{-4}$ – $10^{-5}$  are observed.

Water can be formed in three different ways. At low temperatures the major route of gas-phase production is the *neutral-ion process* and involves a chain of hydrogen-abstraction reactions terminated by dissociative recombination:



The gas-phase *neutral-neutral reaction* is efficient at temperatures above 400 K, with the major sequence:



where the temperatures involved are the energy barriers. In warm gas nearly all the available oxygen is converted into water due to these fast reactions, on a timescale of about one hundred years, and produces about 100 times more water than the neutral-ion process is able to.

The third path of water production is *grain surface hydrogenation* and produces large amounts of water ice on the dust grains, which is believed to be a major reservoir of oxygen. At temperatures above 90 K this ice can sublime to gas-phase water.

Figure 1.1 shows the lower part of the *ortho*-H<sub>2</sub>O energy level diagram. An *ortho* and *para* H<sub>2</sub>O energy level diagram including much higher energy states can be found in Rydbeck & Hjalmarsen (1985). The rotational ground state transition  $1_{1,0}$ – $1_{0,1}$  at 557 GHz is marked, as well as other important molecular lines observed by the Odin satellite. Asymmetric tops with identical hydrogen nuclei, like water, are for symmetry reasons divided into two subspecies called *ortho* and *para* states. The dipole selection rules allow the rotation quantum number  $J$  to change by 0 or  $\pm 1$ , while the quantum numbers  $K_{-1}$  or  $K_{+1}$  can change by  $\pm 1$  or  $\pm 3$ . The states with even  $K_{-1}$  and odd  $K_{+1}$  are called *ortho* states, and vice versa for the *para* states. No transitions between the *ortho* and *para* states are allowed. The degeneracy is three times greater for the *ortho* states, owing to the nuclear spin statistical weights of the hydrogen nuclei.

Water has a relatively large dipole moment, and this implies that many transitions have large A-coefficients (read more in Appendix A). Higher levels are

therefore difficult to populate collisionally. The rotational ground state transition  $1_{1,0}-1_{0,1}$  of *ortho*-H<sub>2</sub>O has A-coefficient  $3.5 \times 10^{-3} \text{ s}^{-1}$ . With a collisional de-excitation rate of  $2.0 \times 10^{-10} \text{ cm}^{-3} \text{ s}^{-1}$  at a kinetic temperature of 20 K, the critical density is  $2 \times 10^7 \text{ cm}^{-3}$ . Most molecular clouds have densities much less than this. At low densities the water rotational levels can still be excited by infrared continuum photons from heated dust grains. Due to the large A-coefficient the optical depth (Appendix A) will be very high for many transitions including the ground state rotational transition observed by the Odin satellite.

The high optical depth of the *o*-H<sub>2</sub>O line precludes a correct abundance estimation. As substitutes, observations of the optically thin *o*-H<sub>2</sub><sup>17</sup>O and the almost optically thin *o*-H<sub>2</sub><sup>18</sup>O transitions are used for column density and abundance determinations (details in Appendix A).

## 1.4 Molecular environments

There are many different molecular environments in the ISM, with distinctive chemical characteristics and intimately linked to the formation and evolution of stars. During a star-formation process the chemical state of the region will be modified by the increasing temperature of young embedded stars (from 10 K to a few 100 K), outflows and shocks that can elevate the temperature locally to more than 2000 K. This high temperature changes the chemical reactions, and also returns material to the gas-phase from the icy dust grains through evaporation. The evaporated species can have been formed previously in the gas-phase and then frozen out onto the dust grains, or through chemical reactions on the surface of dust grains, e.g. the H<sub>2</sub> molecule. Cold gas-phase chemistry can easily produce simple species such as CO, N<sub>2</sub>, C<sub>2</sub>H<sub>2</sub>, C<sub>2</sub>H<sub>4</sub> and HCN, and other simple carbon chains. These molecules can later condense onto dust grains, where subsequent reactions produce such species as CH<sub>3</sub>OH and CO<sub>2</sub>. Sublimation releases the molecules back to gas-phase, where they in turn can act as precursors for larger species.

The transformation of chemical composition in a protostellar nebula will be small in the outer cooler part, but in the inner warm part a major reprocessing of grains and molecules will occur. One important question concerns how much of the organic material present in comets is pristine interstellar material, and to what extent it has been processed within the nebula from it was formed.

Close to stars radiating in ultraviolet, the gas will be ionised in *HII* regions. Farther away there will be a transition region between the ionised gas and the cold and dense cloud, a *Photo Dissociation Region* (PDR). *Shocks* and *outflows* produced by a new-born or a dying star, as well as *Hot Cores* also play important roles in astrochemistry. All these regions represent different stages in the star-formation history. The abundance and distribution of molecules will

probe these different environments. If the chemical evolution of molecules can be understood, they can trace these specific physical activities in the protostellar environment, so that our understanding of star-formation increases. This is done by comparing observations with experimental data and detailed, very complex modelling, taking into account thousands of chemical reactions and reaction rates.

However, the reverse is also true – the initial molecular abundances and level of ionisation affect the star-formation process, including the rate of collapse, and the efficiency of star-formation in the cloud (see chapter 2). Hence the chemistry controls the evolution of molecular clouds and stars, *and* is a diagnostic of the physical conditions in them.

A short summary follows for a few different molecular environments which are relevant for the research presented in later sections.

### 1.4.1 HII regions

Massive and very hot newly-formed O or B-stars radiate large amounts of ultraviolet radiation ( $h\nu > 13.6$  eV), and dissociate and ionise the surrounding molecular and neutral hydrogen isotropically. These fully ionized clouds are signposts of massive star formation and their distribution across our Galaxy indicates that the formation of massive stars is concentrated in the spiral arms of dense gas. The gas is heated to temperatures around 10 000 K, which will cause the hydrogen to emit radiation in visible light. Another name is emission nebulae. One of the best studied examples is the Orion Nebula.

An HII region can be quite large. A star of spectral type O can ionise a region up to hundreds of parsecs in diameter (depends on the density of the star), while a B star will produce a few parsec region. However, these luminous and very massive stars cannot maintain the UV flux for more than a few millions of years, since they have rather short lifetimes.

### 1.4.2 Photodissociation or Photon Dominated Regions

Farther away from a luminous UV-radiating massive star, when the photons have energies between 6 and 13.6 eV (FUV photons), there is a transition zone called photo dissociation region (PDRs) between the ionised HII region, and the dark cold molecular cloud. The FUV photons dominate the physical and chemical processes in a PDR, thus a large portion of the gas in the ISM resides in PDRs. The structure is determined by the density and the intensity of the incident FUV radiation field.

Most high-energy photons are absorbed by the dust and molecules in the outer layers of the PDR, but a small fraction is able to heat the gas by the photoelectric effect to a few hundred K, and to ionise atoms and to dissociate the

molecular species. Photoelectric heating is most efficient in the outer parts below a visible extinction of about six magnitudes. This heats the dust grains which radiate strongly in infrared. A second heating source is photopumping of  $\text{H}_2$  followed by collisional de-excitation. Deeper in the cloud cosmic rays are the main heating source. Cooling occurs mostly from fine-structure lines of abundant atoms and ions, such as [CII] at  $158 \mu\text{m}$ , and [OI] at  $63 \mu\text{m}$  (more in Sect. 2.2). Deeper in the cloud neutral atoms and molecules form subsequently in order of their ionisation and dissociation energies. At the edge of the PDR, where the temperature can be thousands of Kelvin, there is a thin transition region ( $\Delta A_V \simeq 10^{-2}$ ) where UV photons with energies larger than 13.6 eV are absorbed, and the hydrogen atoms changes from being almost fully ionised to almost fully neutral. The remaining FUV photons will dissociate molecular hydrogen and ionise carbon, forming the next region with  $\text{H}^+/\text{C}^+$ . At a visual extinction larger than approximately two magnitudes, the flux of dissociating  $\text{H}_2$  photons is attenuated, and the composition is dominated by  $\text{H}_2$ . CO is forming at  $A_V \simeq 4$  magnitudes, when the ionised carbon recombines. The PDR ends at the O/ $\text{O}_2$  boundary ( $A_V \simeq 30$  magnitudes).

In a PDR, gas-phase water probably exists only within a relatively narrow region near the cloud surface. Closer to the surface than a few  $A_V$ , water is photo-destroyed by the UV-radiation, and deeper in the cloud it depletes onto grains. The highest gas-phase water abundance is therefore found between  $A_V=2$  and 4–8.

Interesting examples are the S140 PDR and the Orion Bar and extended PDR, which is the interface PDR between the Orion KL molecular cloud and the M42 HII region (Wirström et al. 2006).

### 1.4.3 Hot cores

Hot cores are warm ( $T \sim 100\text{--}400 \text{ K}$ ), dense ( $n \sim 10^6\text{--}10^8 \text{ cm}^{-3}$ ) and rather small regions (diameter  $\lesssim 0.1 \text{ pc}$ ). They can be found close to young stars, and could be an early stage to a HII region. The warm environment gives rise to a complex and rich chemistry with a different chemical composition than in the cold and dark clouds. The abundances of saturated (hydrogenated) molecules such as  $\text{NH}_3$ ,  $\text{H}_2\text{O}$ ,  $\text{H}_2\text{S}$ ,  $\text{CH}_3\text{OH}$ , and  $(\text{CH}_3)_2\text{O}$  are very high. In Hot cores there is also an enhancement in the abundance of deuterated species, but there are few molecular ions which suggests a low ionisation. When the temperature is rising molecules evaporates from the ice mantles covering the dust grains. In the gas-phase these molecules can form other complex species. Also, the high temperature allows for reactions with a barrier (endothermic reactions), e.g. the neutral-neutral reactions forming water.

The Orion KL nebula has a well studied Hot core (read more in chapter 4.2 and in papers I and II).

#### 1.4.4 Shocks and outflows

A shock occurs whenever a disturbance through the medium has a speed greater than the speed of sound, which is about  $1 \text{ km s}^{-1}$  in a neutral gas with temperature below 100 K. The energy of a shock with about  $30 \text{ km s}^{-1}$  speed (continuous C-shock), or from energetic outflows from a protostar can elevate the temperature to thousands of K, and this changes the chemistry in the ISM. In the stronger J-shocks (Jump shocks) the temperature can be as high as 10 000 K. At these high temperatures, neutral-neutral reactions are very efficient, even for those with high activation barriers.

The water molecule is rapidly produced in these conditions, converting all neutral atomic oxygen to  $\text{H}_2\text{O}$ . Molecules from dust grains and even grain core material are released by sputtering. If the shock speed is too high (above  $100 \text{ km s}^{-1}$ ), the molecules will dissociate.

The sources of shocks include the interaction of Supernova-Remnants with molecular clouds, cloud-cloud collisions, or molecular outflows from newly born stars.

During the very early stages of a protostar, when it is still embedded inside the parental cloud, *outflows* will be seen (Shang et al. 2006 and references therein). On large scales typically bipolar molecular outflows are seen. They often have low-velocity (few tens of  $\text{km s}^{-1}$ ) and high masses (solar mass scales). This suggests that it is molecular cloud material that is swept up by powerful winds emerging from the new-born star.

#### 1.4.5 Cold dark clouds

The cold ( $\sim 10 \text{ K}$ ) and dark clouds ( $n \sim 10^3 - 10^5 \text{ cm}^{-3}$ ) have mostly molecular gas with  $\text{H}_2$  as dominant species. Due to the high density there is no penetration by visible or UV photons, and the ionisation is low. The chemistry is driven by cosmic rays that penetrate deep into the clouds producing the necessary ions for a neutral-ion driven chemistry.

Over 60 molecules have been detected in these regions (mostly with radio astronomy). Here the largest molecules are found in the form of unsaturated carbon chains (e.g.  $\text{HC}_7\text{N}$ ,  $\text{HC}_9\text{N}$ , and  $\text{HC}_{11}\text{N}$ ).

The masses range from about 1 to  $500 M_\odot$ , with size between  $\sim 1-5 \text{ pc}$ . These clouds can typically form one or two low-mass ( $\lesssim 2 M_\odot$ ) stars.

#### 1.4.6 Giant Molecular Clouds (GMCs)

The majority of all stars form in these very large molecular gas clouds. They are able to form thousands of low-mass stars and several high-mass stars which cannot form elsewhere. Once a GMC has formed, the star-formation starts almost immediately.

GMC's are the most massive individual objects in the Galaxy with masses from about  $10^4$ – $10^6 M_{\odot}$ , and a mean density from about 100 to  $1\,000\text{ cm}^{-3}$ . More than half the total gas mass in the Galaxy is found in GMC's. Their sizes are about 50 pc, but some are elongated with an extent of 100 pc. Their lifetimes are about  $10^7$  years. Once a bright O star is formed the destruction of the GMC will start due to the intense emission of UV radiation which dissociates and ionises the molecules and atoms. Since GMC's are typically found in the spiral arms this implies also that the lifetime cannot be longer than the travel-time across a spiral arm, which is about 50 millions of years.

The internal pressure is about ten times higher than the pressure of the ambient ISM. This suggests that they are self-gravitating objects, i.e. they are held together by the mass of the molecular gas within them, otherwise they would fall apart in about 10 million years.

The internal structure is inhomogeneous with fragments in dense sheets, filaments, cores and large low-density voids. Clumps of higher than average density gas fill  $\sim 5$ – $10\%$  of the volume of the cloud, and in their very densest central parts the most tightly gravitationally bound clumps form stars. Most of the gas in GMCs is thus inactive/sterile.

About 100 molecular species have been detected in GMCs. Examples of GMCs or GMC complexes are the Orion Molecular Cloud, Sagittarius, and the Eagle Nebula.

## Chapter 2

# Star-formation

### 2.1 Jeans mass and star-formation

The standard theory of star-formation describes the gravitational collapse of a cold (10-120 K) and dense cloud core. The forces taken into account are gravity, and the opposing thermal pressure. A cloud of gas will collapse under the influence of gravitation if the mass of the cloud exceeds the *Jeans mass*

$$M_J \simeq \left( \frac{5k_B T}{G \mu m_H} \right)^{3/2} \sqrt{\frac{3}{4\pi \rho_0}} \quad (2.1)$$

Here  $k_B$  is the Boltzmann constant,  $G$  is the gravitational constant,  $T$  is the local temperature of the cloud,  $\mu$  is the mean molecular weight,  $m_H$  is the hydrogen mass, and  $\rho_0$  is the mean density of the cloud. This equation shows the importance of low temperature and a high density, thus in the small cores inside the GMCs star-formation will most naturally occur. Eq. 2.1 also implies the importance of cooling to keep the temperature and pressure low enough not to stop the gravitational contraction (see Sect. 2.2).

The collapse starts with a *free-fall* phase with an almost constant temperature (iso-thermal phase), and is characterized by a free-fall time

$$t_{ff} = \sqrt{\frac{3\pi}{32} \frac{1}{G \rho_0}} \quad (2.2)$$

Note that this time is independent of the initial radius of the cloud, which is assumed to be spherical. For a cloud of initial density of  $10^{-19} \text{ g cm}^{-3}$ , and a temperature of 10 K, the free-fall time is around  $2 \times 10^5$  years.

The rate of mass infall near the core's centre is given by

$$\dot{M} \approx \frac{a^3}{G} \sim \frac{T^{2/3}}{G} \quad (2.3)$$

where  $a$  is the sound speed which is proportional to the square root of the temperature. The equality holds to within an order of a magnitude. Thus the predicted infall mass rate does not depend on the initial cloud density, but only on the temperature. Since a cloud of a fixed mass with higher density has a shorter free-fall time (Eq. 2.2), the accreted mass will be smaller.

This gravitational collapse scenario explain the formation of stars, but the actual details of the event depend on the physical conditions in the star-forming regions. This also determines the mass of the resulting star, and if a double star or a planetary system will be formed. From observations we know that stars have masses between 0.08 to  $\sim 100 M_{\odot}$ , where most of the stars are small, and about half of all stars are double star systems. The star-formation rate per unit mass varies a lot within our Galaxy, but in total is  $\sim 2-3 M_{\odot} \text{ year}^{-1}$ .

However, if the Galaxy contains about  $10^9 M_{\odot}$  molecular gas, and most of the gas is residing in GMC's which are gravitationally unstable, this should produce a star-formation rate higher than about  $200 M_{\odot}$  each year. Since the observations shows about a hundred times lower rate, this suggests that an additional force is counteracting the gravitational collapse.

This force is caused by the magnetic fields which permeate and give support to the clouds. In order for gravitational collapse to start, the gas cloud must first lose its magnetic support. This is done with ambipolar diffusion which is the drift of neutral relative charged particles. The magnetic field is only acting on the charged particles, while the neutral particles that carry most of the mass are affected by the inward gravitational force. If the ionisation is high, the time for the neutral species to drift inwards through the ion gas will be longer than in the case of low ionisation. The effectiveness of a cloud collapse is therefore governed by the fractional ionisation in the cloud, which in turn is controlled mainly by cosmic rays deep into clouds.

The actual onset of a collapse could be triggered by collisions between clouds streaming across a spiral arm, leading to compression to higher densities.

## 2.2 Heating and cooling

As governed by thermodynamics, the temperature inside a collapsing cloud will rise. For a rapid collapse to occur, this thermal pressure support must be kept low by cooling. As long as the cloud is optically thin and has effective *coolants* which can radiate away the gravitational potential energy that is released during the collapse, the temperature can be kept almost constant and the collapse will be prompt. However, if no coolants are available or are inefficient, the cloud will be heated according to Eq. 2.1, which leads to a higher Jeans mass and the collapse will stop.

Heating and cooling occur by a variety of processes, with radiation as the

dominant transport mechanism. If matter is exposed to a radiation field it can extract energy and is heated (see Appendix A). When a high-energy photon ionises an atom or molecule, the kinetic energy of the electron will be the difference of the photon energy and the ionisation energy. The electron will share this kinetic energy with other gas particles through collisions, and thus the gas will become hotter. Cosmic rays are another heating source, which can reach deep into dense and dark clouds where radiation is blocked by molecules and dust particles.

Cooling occurs when ionisation or excitation in an atom or molecule is caused by a collision, and is de-excited by a radiative transition before another collision occurs (see Appendix A). The kinetic energy in the gas is then transferred to radiation that escapes the cloud, which therefore is cooling. Atomic hydrogen is very effective in cooling gas to temperatures around 10 000 K. At lower temperatures there are too few collisions that are able to ionise or excite the hydrogen atoms and the cooling stops.

To be an efficient coolant a species must have a high abundance and have excitation levels comparable to the average kinetic energy in the cloud. This is why molecular clouds are colder than atomic gas. Molecules have more available very low energy levels as compared to atomic transitions. Well-known molecular gas coolants are CO, C, H<sub>2</sub>O, OH, and H<sub>2</sub>, with CO as the most important coolant at low densities. The first excited rotational level of *p*-H<sub>2</sub> has an upper state energy of 510 K, OH has  $E_u = 120$  K, *o*-H<sub>2</sub>O has  $E_u = 27$  K, C has  $E_u = 24$  K, while the lowest level in CO is only 5.5 K above the ground state. In addition CO has closely spaced rotational levels, is easily excited, and is the second most abundant molecule after H<sub>2</sub>. Thus cooling by CO produces very low gas temperatures in molecular clouds. At a density of  $n(\text{H}_2) = 10^3 \text{ cm}^{-3}$ , the isotopologue <sup>13</sup>CO starts contributing to the cooling. Despite the much lower abundance (about 40-70 times lower than <sup>12</sup>CO), the <sup>13</sup>CO and <sup>12</sup>CO cooling can be of the same order, because the latter is optically thick and the emitted photons are re-absorbed. Water becomes increasingly more important as a coolant with higher density and temperature, due to the high dipole moment. At temperatures above 300 K, water is the dominant coolant. At high temperatures and low densities, H<sub>2</sub> is the dominant coolant, while generally unimportant below 100 K.

Other criteria for efficient cooling agents are a high probability for excitation during the collision. The Einstein A-coefficient should be large to guarantee a decay occurring before a second collision. The cloud also need to be optically thin at the frequency of the emitted photon – otherwise the photon will be trapped and re-absorbed within the cloud.

For diffuse clouds with higher temperatures and PDR's, the most important coolants are fine-structure transitions of [CII] at 158  $\mu\text{m}$  ( $E_u = 92$  K), [OI] at 63  $\mu\text{m}$  ( $E_u = 228\text{K}$ ), and [SiII] at 35  $\mu\text{m}$  ( $E_u = 414$  K).

### 2.3 The first stars

The gas in the Early Universe mainly consisted of neutral hydrogen and helium, with trace amounts of deuterium and lithium. Efficient molecular hydrogen production needs the surface of dust grains since two colliding hydrogen atoms cannot associate directly. But in the Early Universe no dust grains were available for molecular production. Instead it was the small ionised fraction of the gas, that gave two important, but rather inefficient and indirect ways to form  $H_2$ . The first one uses an electron as a catalyst. In the first step the electron attaches itself to an H atom to form the negative ion  $H^-$  (radiative association). When this ion collides with an H atom the electron will carry away energy and  $H_2$  will form. The second route involved protons instead of electrons in the same way. A proton and a H atom radiatively associate to form  $H_2^+$  by charge transfer. Another collision with an H atom will produce  $H_2$ , while the energy will be carried away by the proton. The formation by electrons as catalysts is more efficient than by protons, but still none of the two processes is very efficient. Furthermore, the produced  $H_2$  was easily destroyed by radiation and energetic collisions with hydrogen atoms. The resulting  $H_2$  density was about one or two molecules per million of H atoms. Even so, this low abundance was very important. And since there was deuterium present in the primordial gas, HD was also produced with an abundance of about one molecule of HD to  $10^5$  of  $H_2$ . HD is found to be the main cooling agent at temperatures around 200 K.

The presence of these molecules was crucial for the necessary cooling during the star-formation process, and made cooling to temperatures around 100 K possible. But still only a few species with very low abundances were present and the collapsing clouds were inefficiently cooled. As a consequence, the first generation of stars, called Population III stars, were very massive and hence very short-lived. But these stars produced the elements carbon, nitrogen, and oxygen. When these stars experienced a violent death as supernovas, they seeded the Early Universe for the first time with trace amounts of these elements. Thus, the pregalactic gas gradually became more enriched with other elements than hydrogen and helium, and therefore a wider variety of stars could form, i.e. the masses of the stars could be lower because of the more efficient cooling.

The first Population III stars are believed to have formed at  $z=10-20$  (Choudhury & Ferrara 2006).

## Chapter 3

# Searches for Primordial Molecules in the Early Universe

### 3.1 The beginning

Before about 13.7 billions years ago nothing existed. And then in a process called the Big Bang, our Universe – both the space itself and the matter within it — was created. The beginning was extremely hot, but the Universe was, and still is, expanding and therefore cooling. After about 225 s the temperature had dropped to about  $9 \times 10^8$  K, and the existing nucleons (protons and neutrons) could combine into helium, and trace amounts of lithium. In the Standard Big Bang Nucleosynthesis model this was over approximately 3 minutes after the Big Bang, and about 75% by mass was then ionised hydrogen and 25% helium. By number: for each  $10^{12}$  H atoms –  $7 \times 10^{10}$   $^4\text{He}$  atoms was formed,  $4 \times 10^7$  D atoms (i.e.  $^2\text{H}$ ),  $7 \times 10^6$   $^3\text{He}$  atoms, and only 150 Li atoms. The temperature was still high at the time, and no neutral atoms could exist. Instead a plasma of ionised atoms and electrons existed in a thermal equilibrium with the photons. The temperatures of matter and radiation were the same. But due to the expansion of space the radiation became less and less energetic. At a certain time (approximately 300 000 years after the Big Bang) the temperature had cooled to about 3 000 K. This is the time of *recombination*, and the protons could now combine with the electrons and produce neutral hydrogen.

When this happened the close thermal coupling between the matter and radiation (previously maintained by Compton scattering of photons and electrons) was lost. From this time forward the temperatures for matter and radiation evolved separately. Thus at the time of *recombination* the Universe became transparent to the existing photons which today can be seen as the Cosmic Microwave Background (CMB). The CMB radiation has been observed by sensitive radiometers on the two satellites COBE and WMAP, and shows the small density/temperature fluctuations from the recombination epoch.

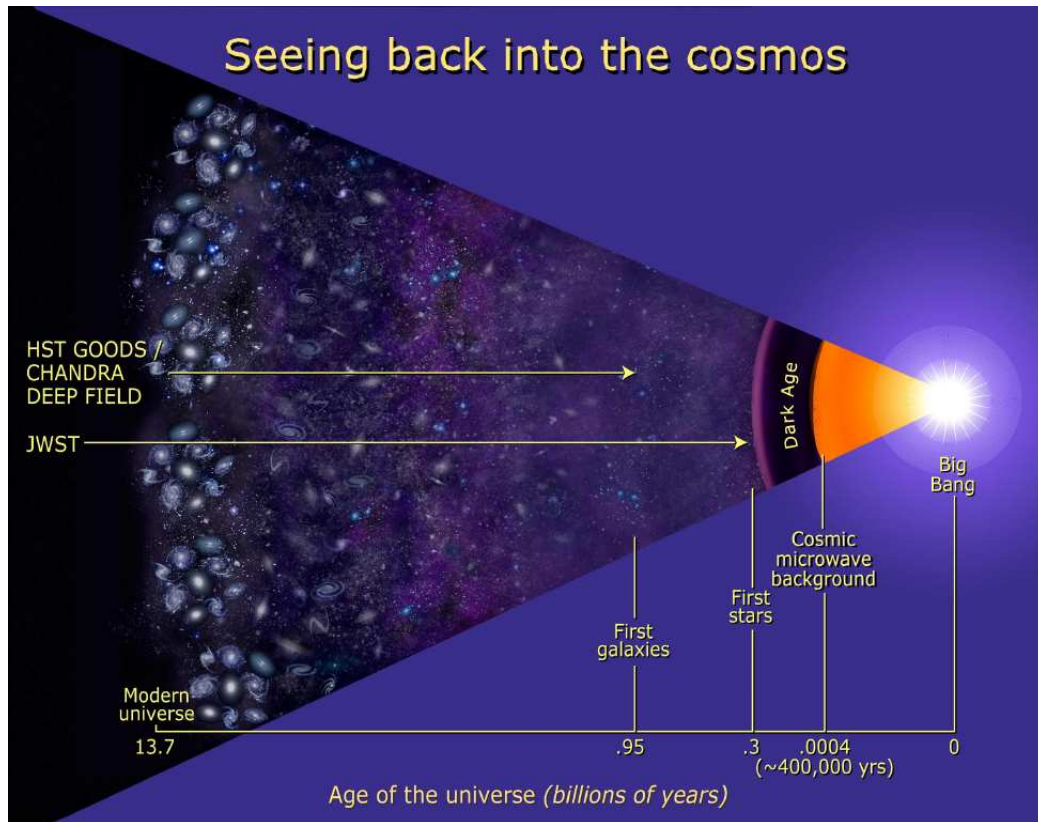


Figure 3.1: The history of our Universe; from the Big Bang, via the Dark Ages, the formation of the first stars and galaxies to today. Credit: NASA and Ann Field (STScI).

After the recombination the Universe became dark. The cosmic *Dark Ages* began and did not end until the formation of the first stars (Pop III) and galaxies. During this time the transition from the small density fluctuations left over from the Big Bang to the strong non-linear structure we observe today took place. We observe stars, and galaxies on large scale in a structured form of large filaments between large voids. But still, there is no good understanding of how the first stars were produced, or how galaxies and clusters formed. We observe the CMB radiation and obtain information from the recombination epoch. And then we model a theoretical evolution from the recombination epoch to the structure observed today, and try to fit the observations. Models predict that the first stars were very massive and short-lived, and appeared between 100 and 250 million years after the Big Bang. These stars altered the chemistry in the Universe by producing the first heavy elements, and influenced the dynamics by heating and ionising the surrounding gas.

One of the remaining big unanswered questions in astronomy is illustrated in Fig. 3.1:

- *Origin of structure.* How did the Universe evolve from the near uniformity at the recombination to the structures of clusters, galaxies and voids that we observe today during the epoch of the Dark Ages?

Direct observations from the cosmic *Dark Ages* are most commonly believed to be impossible. But our aim in the search for the *Primordial molecules* is to do exactly this – from an initial idea of Dubrovich (1977) as amplified by Zel’dovich (1978) – to perform observations of resonant spectral lines from cloud structures evolving during the cosmic *Dark Ages*.

### 3.2 Elements of our primordial medium

We start our investigation of the *Dark Ages* by an inventory of its constituents:

- *Atoms/ions and electrons.* After the time of the recombination most species were the neutral H, D, He and trace amounts of Li. The recombination was sequential in the order of the ionisation potentials, beginning with  $\text{Li}^{3+}$  and ending with  $\text{Li}^+$ . Hydrogen became neutral at  $z \sim 1100$ , and helium already at  $z \sim 2500$ . However, the recombination was not instantaneous, and since the Universe expanded and cooled faster than recombination was completed, a small fraction of free electrons and protons remained. For this reason, the recombination of  $\text{Li}^+$  was not completed.
- *CMB photons.* The existence of the Cosmic Microwave Background (CMB) radiation was first predicted by George Gamov in 1946, Alpher and Herman in 1949. The discovery in 1965 was inadvertently made by Arno Penzias and Robert Wilson who shared the 1978 Nobel prize in physics for their discovery. After many attempts with ground-based and balloon-borne observations, it became clear that the measurements needed to be done from space above the Earth’s bright and obscuring atmosphere (the CMB spectrum peaks at 2 mm). NASA’s Cosmic Background Explorer (COBE) satellite was launched on 18 November 1989. The first result, only nine months afterwards, was the most perfect blackbody radiation ever observed and supported the Big Bang theory. Moreover the CMB showed density (equivalent to temperature) fluctuations of the order of  $1/100\,000$ . At the time of recombination the temperature was about 3 000 K, while observed today only 2.73 K. The decrease in temperature is due to the cosmological expansion of the Universe. These observations were major achievements and the 2006 Nobel prize in physics is awarded to John Mather and George Smoot, who were in charge of these measurements. The Wilkinson Microwave Anisotropy Probe (WMAP) was launched in June of 2001 to continue to map the CMB temperature fluctuations with higher resolution,

sensitivity, and accuracy than COBE. In February 2003 WMAP released results from the first year of flight data (Bennett et al. 2003), and the third year results are available since March 2006 (Spergel et al. 2006).

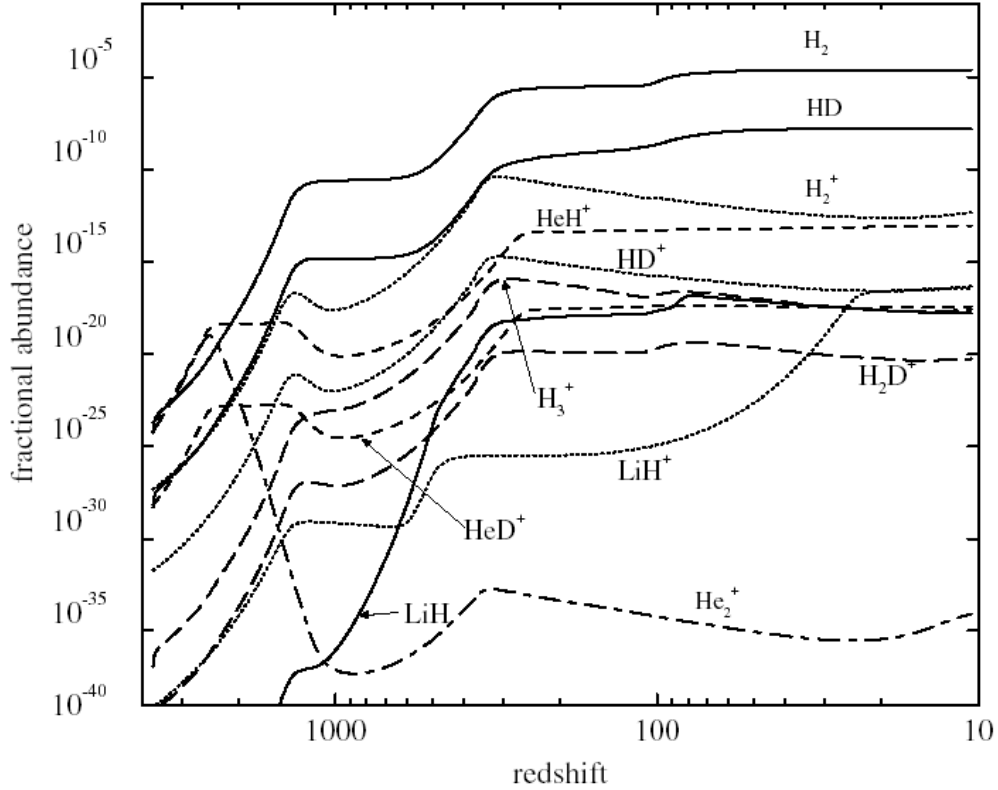


Figure 3.2: Fractional abundances in the Early Universe of molecules and ions as a function of redshift  $z$ . The calculations assume cosmological parameters  $\Omega_0 = 1$ ,  $\Omega_b = 0.0367$  and  $h = 0.67$ . Credit: Lepp et al. 2002.

- *Molecules.* When the temperature in the Universe had dropped sufficiently the production of molecules started. Even though the BB models produce only three elements and a few isotopes, a surprisingly complicated chemistry emerges. About 200 reactions contribute to the abundance of 23 atomic and molecular species which might be important in the early Universe. But the resulting abundances are highly uncertain due to difficulties to compute or measure all the reaction rates in the typical conditions in the early Universe. Also cosmological parameters affect the production of molecules. If a dark energy is incorporated in the models by invoking a decaying cosmological constant the matter temperature will decrease much faster. This would shift molecular formation to a much earlier epoch, and the limiting abundance of  $H_2$  would be doubled. Based on a Standard Big

Bang Nucleosynthesis model, Fig. 3.2 shows the evolution of the fractional abundances of the molecules as functions of redshift  $z$ . This is one of the more recent models from Lepp et al. (2002).

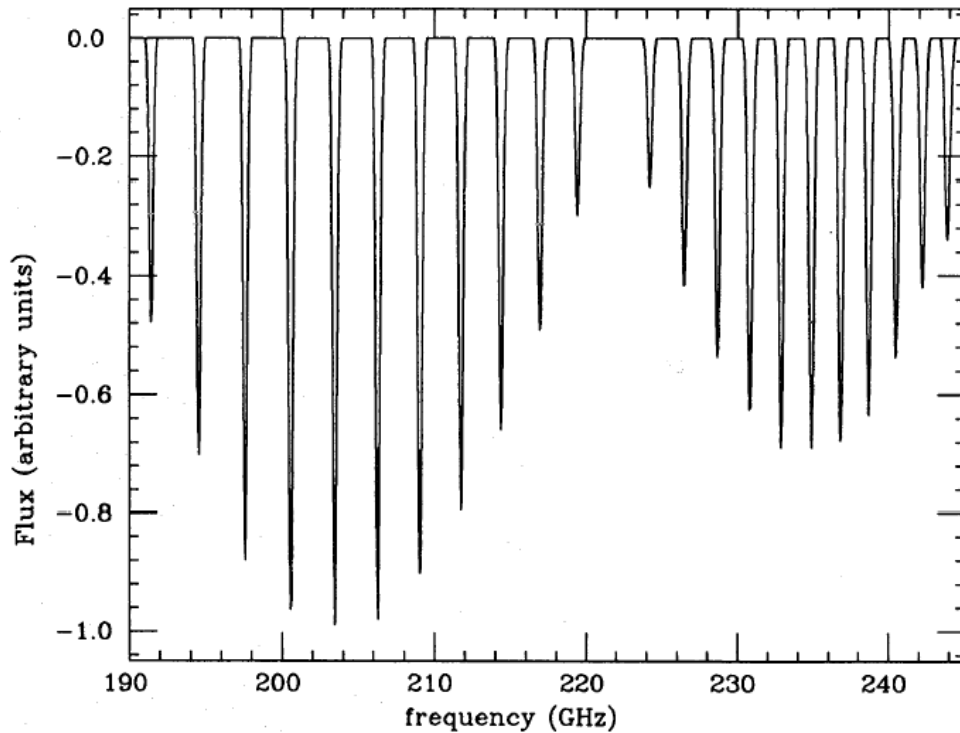


Figure 3.3: Rotational-vibrational lines for LiH, arbitrary intensity scale. Credit: de Bernardis 1993.

### 3.3 Resonant scattering

Since the densities of the elements are very low, absorption and emission processes are ineffective. The most efficient process to couple the CMB photons with molecules, ions, and atoms is resonant scattering. In this process a photon is first absorbed and then re-emitted at the same frequency, but not in the same direction (elastic scattering). The cross-section for this scattering is several orders of magnitude larger than the Thompson scattering between the CMB and electrons.

This scattering does not alter the CMB spectrum, but it could smear out the primordial spatial distribution of the CMB and produce secondary anisotropies. However, since the CMB is a diffuse background, scattering is not enough to

produce a signal – a peculiar velocity for the scattering source is also needed, i.e. a source velocity that is not from the cosmic expansion.

The optical depth for the transition depends on the product of the abundance and the dipole moment of the considered species. Due to the frequency dependence of the cross-section, rotational or ro-vibrational lines will appear. Figure 3.3 shows rotational-vibrational transitions for LiH with an arbitrary intensity scale (de Bernardis et al. 1993).

$$\tau_{ij} = \int_{\text{source}} \sigma_{\text{res},ij} n_i ds \sim 3.37 \cdot 10^{-19} \int_{\text{source}} |\vec{d}|^2 \frac{\nu_{ij}}{\Delta\nu} n_i ds \quad (3.1)$$

where  $\sigma_{\text{res},ij}$  is the cross-section for the resonant scattering,  $n_i$  is the density of the species in state  $i$ ,  $\nu$  is the frequency of the transition,  $\Delta\nu$  is the width of the line, and  $d$  the dipole moment of the species.

The lines can be emission- or absorption-like depending on the sign of the radial peculiar velocity of the primordial cloud. The line width and intensity depend on the dynamics of the primordial clouds which can be divided into three different phases:

- *Linear evolution.* The perturbation in the primordial gas clouds follows the Hubble expansion of the Universe. Within the cloud different parts will fulfil the conditions for resonant scattering for different redshifts. Hence the line-widths will be very broad and the signal very weak, since they depend on the extension in redshift of the perturbation, i.e. mass and redshift.  $\Delta\nu/\nu$  can be as high as 0.01 for a  $10^{14} M_{\odot}$  perturbation at high  $z$ .
- *Turn-around phase.* At this moment the gravitational force in the primordial gas clouds matches exactly the Hubble flow and the cloud appears to be non-moving. All the scattered photons will contribute to the signal at the same frequency. This will produce the narrowest and strongest signals, where the line width is due to thermal broadening ( $\Delta\nu/\nu \sim 10^{-6}$ ).
- *Non-linear collapse.* The gravitational collapse of the primordial clouds begins. The line shape will depend on the ratio of the peculiar velocity and collapse velocity.

The most favourable regimes for detections are during the turn-around phase and the non-linear collapse.

When we observe a moving source the observed lines will be redshifted as

$$\nu_{\text{obs}} = \frac{\nu_0}{1+z} \quad (3.2)$$

where  $z$  is the cosmological redshift, which is a measure of the distance and time we look back in the Universe. This also implies a very low probability

to have more than one source along the line of sight with the same dynamical and molecular conditions. Hence, we are looking for spectral lines emitted from a well defined primordial source at a certain redshift. Increasing the bandwidth will improve the explored redshift range. Another advantage of a broad band width is the possibility to detect several lines of the same species, which is needed to confirm the origin of the line.

The intensity of the lines can be approximated as

$$\frac{\Delta I}{I} \sim \frac{v_p}{c} \tau_{ij} \quad (3.3)$$

where  $v_p$  is the peculiar velocity of the moving cloud.

### 3.4 Implications

The detection of redshifted spectral line patterns from primordial molecules would tell us about:

- The existence of a protostructure at a given  $z$ .
- The chemical composition, peculiar velocity and mass of the primordial clouds via the properties of the line, thus constraining structure-formation models.
- The accuracy of Big Bang Nucleosynthesis models.
- The epoch of first star formation and setting constraints on the time of reionization

The only spectral signature produced before the epoch of the first Pop III stars is the resonant spectral lines. Hence a serious detection attempt should be one of the main cosmological items.

### 3.5 Observations

#### 3.5.1 Previous observations

The only previous observations were made with the IRAM 30 m telescope in 1992 by de Bernardis et al. Seven high-latitude regions were investigated with a 1 GHz band at 3 different frequencies in the 1.3, 2 and 3 mm atmospheric windows where two ro-vibrational bands of LiH are expected from  $z \sim 180$ . No lines were seen, but upper limits (depending on the redshift of the cloud) of the order of 20 mK for the intensity of the LiH lines were calculated.

### 3.5.2 Our Odin observations

When looking for primordial resonant lines, several things need to be considered. A broad band is needed to explore a wide range of redshift, and also to enable observations of several lines from a species to check the origin of the line. Since the lines are expected to be very weak, a low noise-level is also required.

Since the abundance determinations are very uncertain, it is difficult to predict what species and lines we are looking for. Ten years ago, LiH was believed to be the best candidate for a resonant line detection, due to its high dipole moment and the, at the time, believed high abundance of  $\sim 10^{-10}$  after freeze out. More recent models find an abundance of  $\sim 10^{-18}$ – $10^{-20}$ . In this case, a signal will not be possible. Today, HeH<sup>+</sup> is considered as a more interesting species, with an abundance of  $\sim 10^{-14}$  at a redshift of  $\sim 100$ , and a dipole moment of 1.78 Debye. Other interesting species are H<sub>2</sub> with an abundance of  $\sim 10^{-5}$ – $10^{-6}$ , H<sub>2</sub><sup>+</sup> with  $\sim 10^{-13}$ , and HD with  $\sim 10^{-10}$ – $10^{-12}$ .

Satellite observations also have the advantage of the absence of spectral line poisoning by the terrestrial atmosphere.

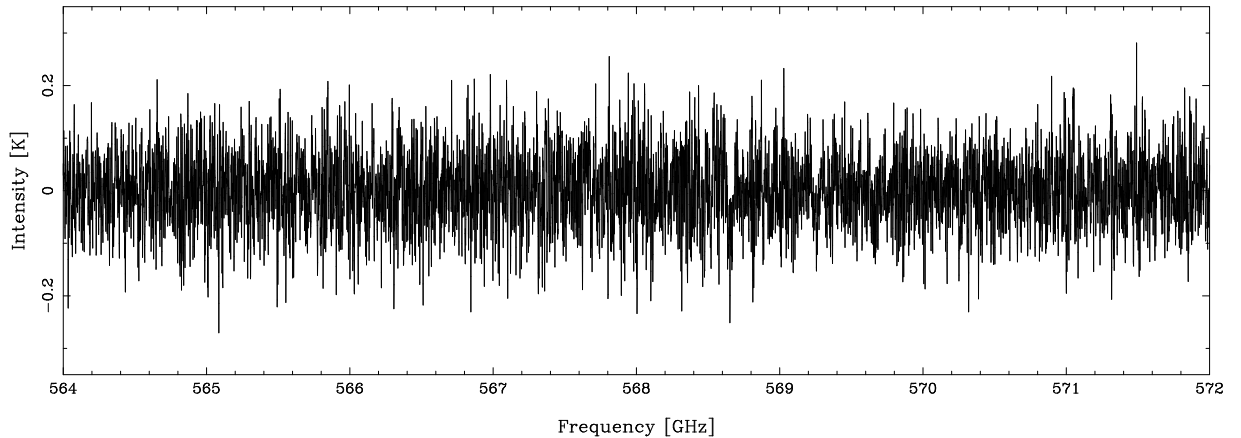


Figure 3.4: Part of spectral line survey towards a WMAP hot spot.

- Already performed observations.

A Swedish-French Odin-team has performed a Spectral Scan with the Odin satellite towards two WMAP Hot Spots (Bennett et al. 2003) during the summer 2004 in the frequency band 547–578 GHz (31 GHz). The resolution is 1 MHz. To cover this wide bandwidth 340 orbits were spent on the observations.

Fig. 3.4 shows part of the 31 GHz spectral scan with a resolution of 1 MHz ( $0.5 \text{ km s}^{-1}$ ). As seen the rms noise level is  $\sim 65 \text{ mK}$ , which was reached by an integration time of each LO setting (i.e. 5 orbits for each setting) of

~3000 s. No lines are detected, but the resulting data set is not yet fully analysed.

Since we do not know the exact width of the resonant lines, the resolution can be increased in steps, gaining a lower noise level.

- Planned observations

The distortions in the CMB background are not only spectral in character but also spatial. The angular size of a primordial cloud at turn-around or during the non-linear collapse can range from arcseconds to many arcminutes. Since the size of the clouds or their redshifts are not known, we have an observational problem. The resulting spectrum from the observations is the difference between an on- and an off-position. If the off-position is too close to an emitting source, a possible signal would disappear.

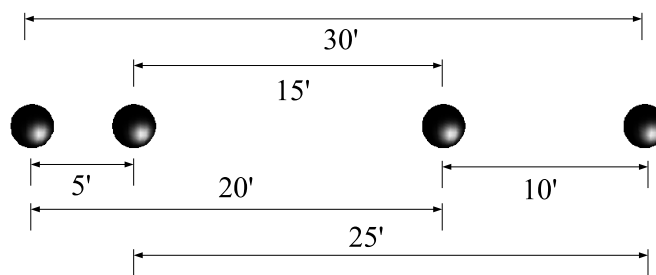


Figure 3.5: Observing strategy for Primordial molecule observations during winter 06/07 with the Odin satellite.

We have therefore developed a new observing strategy for the upcoming Odin observations illustrated in Fig. 3.5. We have been awarded time for new observations with the Odin satellite – 10 full weekends, which means about 430 orbits in total. We will perform a spectral line survey in the frequency ranges 542.0-547.5 GHz and 486.5-492.0 GHz towards four different points, i.e. in total 11 GHz spectral line survey for each position. There are a number of different redshifted lines that can fall into these frequency bands, such as the  $\text{HeH}^+$   $J=1-0$  transition which shifts to 545 GHz at  $z=2.7$ , the  $J=2-1$  from  $z=6.4$ , and the  $\nu=1-0$  R(0) shifts to 545 GHz at  $z=162$ . The position of the first point is the same as used in previous observations, a Hot Spot as detected by the WMAP satellite with coordinates R.A.  $05^h26^m00^s.0$ , Dec.  $-48^\circ30'00''.0$  (J2000). The positions of the second, third and fourth point are 5', 20' and 30' away from the first point in declination. We will have four times more integration time for every setting in this spectral line survey as compared to our previous observations, to lower the noise. In addition we will have six different spacings with observations of only four positions as seen in Fig. 3.5. This will allow us to test

six different combinations of positions and hence sizes of the primordial clouds.

### **3.6 Future prospects**

Our next future step will be to use ESA's Herschel Space Observatory<sup>1</sup>, which is much more sensitive than Odin and also allows coverage of a very large frequency range.

However, what we really would need is a dedicated space mission for this key cosmology project!

---

<sup>1</sup><http://sci.esa.int/science-e/www/area/index.cfm?fareaid=16>

## Chapter 4

# Introduction to Paper I and Paper II

### 4.1 The Odin satellite

The accurate determination of the water and oxygen abundances in the various phases of the ISM poses a severe observational difficulty. Due to the absorption by water and oxygen, the terrestrial atmosphere is completely opaque at frequencies around 119, 487 and 557 GHz. Any observations in these spectral regions have to be done from space or balloon experiments. The Odin sub-millimetre wave spectroscopy satellite is especially designed to solve these problems. And despite the use of advanced technology and the combination of two scientific disciplines on a single satellite – astronomy and aeronomy – Odin is a small, low-cost, and successful spacecraft. The astronomical scientific objectives are to study the water and oxygen chemistry in the ISM and star-formation regions, comets and circumstellar envelopes, while the aeronomers study molecules relevant to ozone depletion. Additional lines from species like ammonia, and carbon monoxide with isotopologues are also observable and can aid the analysis of water and oxygen, .

The Odin satellite was launched on 20 February 2001 by a Start-1 rocket from Svobodny in far-eastern Russia. The orbit is sun-synchronous at an altitude of about 600 km. Odin has successfully been operating for almost six years while the promised life-time was only two years. Nordh et al. (2003) and the subsequent papers in the A&A "Special Letters Edition: First Science with the ODIN satellite" describe the satellite and its first science in detail. More recent progress is discussed by Hjalmarson et al. (2005).

The Odin satellite is a next sensitive step after the SWAS satellite which had a  $3'.3 \times 4'.5$  beam size, and non-tunable receivers (Melnick et al. 2000 and subsequent ApJ papers in that issue). Odin is equipped with an offset Gregorian telescope of diameter 1.1 m, with beam widths of  $2'.1$  and  $10'.0$  at 557 GHz and 119 GHz, respectively. The receiver package is actively cooled to about 140 K and consists of four tunable sub-mm Schottky mixers. The frequency bands

covered are 486–504 GHz and 541–581 GHz. In addition a fixed-tuned HEMT receiver at 118.750 GHz for sensitive O<sub>2</sub> searches was added in the later phase of the extended instrument planning. Any combination of three receivers can be simultaneously used together with a broadband acousto-optical spectrometer (AOS): BW=1 050 MHz, resolution 0.6 MHz, and two flexible hybrid autocorrelation spectrometers (AC1 and AC2): BW=100–800 MHz, resolution 0.125–1 MHz. The main beam antenna efficiency is close to 0.9 which makes the intensity calibration very accurate.

The tunable receivers enable Odin to perform a full spectral line survey in a spectral region previously unobserved, as described in Sect. 4.3 and in Paper I and Paper II.

The Odin satellite addresses several key-questions to be even more accurately addressed by ESA's up-coming Herschel satellite (launch planned early 2008). It will be located at the second Lagrange point (L2) of the Earth-Sun system, and will cover the full far infrared and sub-millimetre wave-band (60–670  $\mu\text{m}$ ) with an order of a magnitude more sensitive SIS mixers and a 3.5 m mirror – the largest civilian mirror ever deployed in space. The Odin science can therefore serve in important pilot studies, as e.g. our current searches for Primordial Molecules and the Odin spectral scan survey of Orion KL.

## 4.2 The Orion nebula

At a distance of only  $\sim 450$  pc, the Orion KL (Kleinmann-Low) region is the closest and most interesting high mass star-forming region, where O and B star-formation is on-going (see Genzel & Stutzki 1989 and references therein for a review). This source is very complex and chemically structured and contains extremely young and massive embedded stars which are not yet visible due to the surrounding dust. It is the brightest infrared region in the  $1^\circ$  large Orion Molecular Cloud OMC-1 complex, situated about  $1'$  NW behind the Trapezium stars in the sword of the Orion constellation. The Trapezium is one of the most famous high-mass star-forming regions. The brightest object is  $\Theta^1$  C Ori, with spectral type O6 and a mass of  $33 M_\odot$ . These stars are situated close to the centre of a dense cluster, where the stellar density near the centre is about 10 000 stars per  $\text{pc}^3$ . About half of the cluster members are optically visible, which is possibly due to the UV-radiating O stars that have cleared away much of the ambient gas. Their intense radiation has ionised the surrounding gas in the M42 HII region in front of OMC-1. The interface between M42 and OMC-1 constitutes one of the famous PDR regions in Orion (Wirström et al. 2003).

The chemical richness in such a star-forming region and its proximity, makes Orion KL an ideal target for spectral line surveys at millimetre and sub-mm wavelengths. And indeed, this is one of the best studied regions of the inter-



Figure 4.1: The Odin beam overlaid on a colour composite image of the central part of the Orion Nebula, M42, also showing the BN/KL region, based on 81 images obtained with the infrared multi-mode ISAAC instrument on the ESO Very Large Telescope (VLT) at the Paranal Observatory (ESO PR photo 03a/01 2001). The red emission at  $2 \mu\text{m}$  comes from shock excited  $\text{H}_2$  caused by a strong bipolar outflow wind from a very young massive star newly born. This is addressed in considerable detail in paper II.

Table 4.1: Angular scales of the Orion nebula at a distance of 450 pc, as compared to angular resolution of different telescopes.

Angular scale of Orion				
Inner solar nebula	Outer solar nebula	Presolar nebula	Cloud core	Cloud
5 AU	100 AU	1000 AU	0.05 pc	0.5 pc
0".01	0".2	2"	23"	4'

Angular resolution at frequencies				
Telescope	115 GHz	230 GHz	345 GHz	810 GHz
ALMA <sup>a</sup>	0.05"–4"	0.02"–2"	0.02"–1.5"	0.007"–0.6"
OVRO <sup>b</sup> , BIMA <sup>c</sup> , IRAM <sup>d</sup>	4–7"	1–2"	–	–
30 m IRAM <sup>d</sup>	22"	12"	7"	–
15 m JCMT <sup>e</sup> /SEST <sup>f</sup>	44"	20"	15"	6"
10 m CSO <sup>g</sup>	–	30"	20"	9"
3.5 m Herschel <sup>h</sup>	–	–	13"–45" at 1600–480 GHz	
1 m Odin <sup>i</sup>	–			126" at 557 GHz

<sup>a</sup>The Atacama Large Millimeter Array (ALMA). <sup>b</sup>Owens Valley Radio Observatory. <sup>c</sup>Berkeley-Illinois-Maryland Array. <sup>d</sup>Institute de Radio Astronomie Millimetrique. <sup>e</sup>James Clerk Maxwell Telescope. <sup>f</sup>Swedish-ESO Submillimetre Telescope. <sup>g</sup>Caltech Submillimeter Observatory. <sup>h</sup>The Herschel Space Observatory; the largest ever IR space observatory when it is launched in 2007. <sup>i</sup>The Odin submillimetre satellite (Sect. 4.1).

action of young massive stars and their parental molecular cloud. Fig. 4.1 shows a colour composite image of the Orion Nebula. The Odin beam is drawn around the central position of our observations, which is the position of the most luminous infrared object in the region Orion KL region, IRC2.

In addition to the chemical structure, the Orion KL region also has a complicated velocity field. In summary the large Odin beam (2.1 arcminutes at 557 GHz) encompasses the following subsources: the bipolar *Low-* and *High-Velocity outflows*, the *Hot Core*, the *Compact Ridge* and *Extended Ridge*, and the extended *PDR* region. They all have different sizes, are situated at different LSR velocities, and have different velocity fields. This will yield lines with characteristic line widths at characteristic LSR velocities from each subregion, which enables an interpretation of the origin of the transitions. In addition, comparison can be made with interferometric data for the small subsources.

But – analysis of a spectral line is not always straightforward. For example the emission from a single molecule is not restricted to one single subregion in Orion KL, but may be the result of a complicated blend from several regions and this leads to complicated line profiles. Thus, when we attempt to derive

column densities and abundances, we have to separate the overall emission into its constituent parts.

Observations have different spatial resolutions (as well as spectral ones) depending on the size of the telescope. This determines what emission will fall into our beam. When observing with a high resolution telescope, or by interferometry, we see emission only from small scales. Everything larger than the beam will not be seen. So a *combination* of observations with high and low spatial resolution is required to perform a complete description of the region of interest. The scale of the studied objects in the Orion Nebula, is illustrated in Table 4.1, both in physical length (pc) and angular scales, along with the spatial resolution of several well known telescopes. As is clearly seen, the required high resolution to observe the smallest inner parts will not be available until the ALMA interferometer is in operation on the high-altitude Llano de Chajnantor (5000 m elevation) in the Chilean Andes<sup>1</sup>. Each of ALMA's movable antenna dishes will measure 12 m wide. The array will measure 150 m to 14 km, and will cover a frequency range from 30 to 950 GHz. The construction of ALMA started in 2003, will become incrementally operational from 2010 on, and is planned to be completed in 2012,

### 4.3 Summary of Paper I and Paper II

A spectral line survey is an ideal opportunity for an unbiased search of new species, and to establish which molecules are present and their abundances in the observed gas. The derived abundances and temperatures are then used to constrain chemical models of molecular production in regions with varying temperature, density and physical conditions such as shocks or outflows.

Many ground-based spectral line surveys have been made of the Orion KL region, at both lower and higher frequencies, but due to the absorption by water and oxygen, the terrestrial atmosphere is completely opaque at frequencies around 487 and 557 GHz. To cover these frequencies we have used the Odin satellite to perform a spectral line survey in the frequency ranges 486–492 GHz and 541–577 GHz, not possible to observe from ground, filling the gaps between previous spectral scans.

After extensive data-reduction work, a long spectrum of total 42 GHz was obtained. The next step was then to decide what features should be called lines – or only noise. When this was done, all the 347 lines needed identifications – if possible. The most important aspect of line identification is to have accurate frequencies of the transitions. We have used several databases for this purpose, such as the SLAIM03 molecular line catalogue<sup>2</sup> available on CD (Lovas 2003),

---

<sup>1</sup><http://www.eso.org/projects/alma/>

<sup>2</sup>Not available on-line, but some of its content is found at <http://physics.nist.gov/PhysRefData/>

the Cologne Database for Molecular Spectroscopy<sup>3</sup> (CDMS, Müller et al. 2001) and the Jet Propulsion Laboratory<sup>4</sup> database (JPL, Pickett et al. 1998) and the Leiden<sup>5</sup> database (Schöier et al. 2005). In these databases frequencies of transitions in these spectral regions can be found, as well as other molecular parameters (upper state energy, transition quantum numbers, A-coefficient or line strength). Unfortunately, these databases are not complete. The spectroscopy still is sparse at higher frequencies and a number of unidentified lines in our survey are likely to be poorly known transitions of the identified molecules and their isotopologues, including their vibrationally or torsionally excited states.

Line identification is not only finding a frequency of a transition that matches the observed feature. Very often, many transitions lie well within the observed line width and are therefore possible candidates of origin. But the chemistry and abundance of a species can suggest an origin of the lines, and as a starting point previously observed species can be considered. The line shape and strength have to be taken into account as well as the presence of other expected line features from the same species. As a first approximation an LTE model is assumed thereby giving the integrated intensities of the transitions from the various upper states.

Some of the results from the Orion KL spectral line survey:

1. We have detected 38 different molecular species with a total of 347 lines.
2. The unidentified lines are 19% of the total. Some tentative assignments of a few of them have been made such as the first interstellar anion,  $\text{SH}^-$ ,  $\text{SO}^+$ , ND and  $\text{CH}_3\text{OCHO}$ .
3. The total emission in our survey is dominated by CO, *o*-H<sub>2</sub>O, SO<sub>2</sub>, SO, <sup>13</sup>CO and CH<sub>3</sub>OH. Species with the largest number of lines are CH<sub>3</sub>OH, (CH<sub>3</sub>)<sub>2</sub>O, SO<sub>2</sub>, <sup>13</sup>CH<sub>3</sub>OH, CH<sub>3</sub>CN and NO.
4. Six water lines are detected including the ground state transition 1<sub>1,0</sub> – 1<sub>0,1</sub> of *o*-H<sub>2</sub>O, and isotopologues *o*-H<sub>2</sub><sup>18</sup>O and *o*-H<sub>2</sub><sup>17</sup>O. A weak line feature at 489.054 GHz is identified as the 4<sub>2,3</sub> – 3<sub>3,0</sub> transition of *o*-H<sub>2</sub><sup>18</sup>O with an upper state energy of 430 K. Hot Core emission from water is observed from the *p*-H<sub>2</sub>O transition 6<sub>2,4</sub> – 7<sub>1,7</sub> with upper state energy 867 K. We have also observed the HDO 2<sub>0,2</sub> – 1<sub>1,1</sub> transition from the Low Velocity Flow and Compact Ridge, and have a tentative detection of the high energy transition (581 K) 6<sub>2,4</sub> – 6<sub>2,5</sub> of HDO.
5. The 1<sub>0</sub> – 0<sub>0</sub> transitions of NH<sub>3</sub> and the isotopologue <sup>15</sup>NH<sub>3</sub> are observed.

---

<sup>3</sup><http://www.ph1.uni-koeln.de/vorhersagen/>

<sup>4</sup><http://spec.jpl.nasa.gov/>

<sup>5</sup><http://www.strw.leidenuniv.nl/~moldata/>

6. Abundance ratios of [D/H], [ $^{12}\text{C}/^{13}\text{C}$ ], [ $^{32}\text{S}/^{34}\text{S}$ ], [ $^{34}\text{S}/^{33}\text{S}$ ], [ $^{18}\text{O}/^{17}\text{O}$ ], and [O/S] are calculated.
7. Different methods are used to obtain rotation temperatures and column densities. For 8 different species which had at least four lines and a sufficient energy range in the transitions, the rotation diagram method is applied. The other methods used as comparison models are the LTE approximation for a single line, and the forward model.
8. Abundances are estimated for the observed species from the different sub-regions, and we find very high gas-phase abundances of  $\text{H}_2\text{O}$ ,  $\text{NH}_3$ ,  $\text{SO}_2$ ,  $\text{SO}$ ,  $\text{NO}$ , and  $\text{CH}_3\text{OH}$ .
9. The number of lines is 4–20 per GHz, with a mean of 8 per GHz. This is comparable with larger telescopes ( $\sim 10 \text{ GHz}^{-1}$ ), showing the excellent performance of the Odin satellite.
10. The apparent noise level is higher than expected from the integration time, which suggests that we are approaching a line forest of unidentified lines (the "confusion limit").
11. A lower limit to the line-to-continuum ratio is 0.2, which is consistent with previous estimations.



# Paper I

A spectral line survey of Orion KL from 486–492 and 541–577 GHz with the Odin satellite.

## I. The Data

To be submitted to *Astronomy & Astrophysics*



# Paper II

A spectral line survey of Orion KL from 486–492 and 541–577 GHz with the Odin satellite.

## II. Data analysis

To be submitted to *Astronomy & Astrophysics*



# Abstract of poster

Progress in searches for primordial resonant lines using  
the Odin satellite

IAU Symposium 231, Astrochemistry: Recent Successes and Current Challenges  
231, 241, 2005



# Appendix A

## Tools of astronomy

### A.1 Radiative transfer

With the equation of radiative transfer we describe how the intensity changes when the radiation travels from a source through a medium towards us. Photons can be *added* to the original beam of radiation from the medium it travels through. They can also be *removed* by scattering or absorption. If no local emission or extinction occurs, the intensity stay constant along the way.

To describe the amount of intensity added by local photon emission to the beam, we use the frequency-dependent *emission coefficient*  $j_\nu$ , which is defined as:

$$j_\nu \equiv \frac{dE_\nu}{dV dt d\nu d\Omega} = \frac{dI_\nu(s)}{ds}. \quad (\text{A.1})$$

This expression describes the energy  $dE_\nu$  that is added in the form of photons to a beam with solid angle  $d\Omega$ , over the bandwidth  $d\nu$ , during a time  $dt$ , within the volume  $dV$ . This is the same as the change of intensity along the travelled path  $ds$ . The dimensions of  $j_\nu$  are [ $\text{erg cm}^{-3} \text{ s}^{-1} \text{ Hz}^{-1} \text{ sr}^{-1}$ ].

The removal of emission from the beam is proportional to the number of extinguishing particles and to the supply of photons. The frequency-dependent proportionality constant is called the *extinction coefficient*, and can be defined per particle, per gram, or per  $\text{cm}^2$ .

$$dI_\nu \equiv -\sigma_\nu n I_\nu ds \equiv \kappa_\nu \rho I_\nu ds \equiv -\alpha_\nu I_\nu ds. \quad (\text{A.2})$$

where  $n$  is the density of the absorbing particles [ $\text{cm}^{-3}$ ],  $\sigma_\nu$  is the effective cross-section per particle [ $\text{cm}^2$ ], and  $\kappa_\nu$  is the monochromatic mass extinction coefficient (the *opacity*, [ $\text{cm}^2 \text{ g}^{-1}$ ]), and  $\rho$  is the mass density [ $\text{g cm}^{-3}$ ], and  $\alpha_\nu$  is the monochromatic linear extinction coefficient [ $\text{cm}^{-1}$ ]. In this section the transport of radiation is described with the extinction per cm,  $\alpha_\nu$ .

Using the emission- and absorption coefficients the change of intensity as it

travels through a medium can be written as:

$$\frac{d I_\nu}{ds} = j_\nu - \alpha_\nu I_\nu. \quad (\text{A.3})$$

This is the *equation of radiative transfer*, and can be used generally except when the absorbing particles are large with respect to their mean distance, or if they are not randomly distributed in the medium.

### A.1.1 Optical depth and source function

To further simplify Eq. (A.3) we use the optical depth concept:

$$d\tau_\nu(s') \equiv -\alpha_\nu ds' \quad (\text{A.4})$$

The total optical depth is obtained by integrating (A.4) over the total path,  $s$ , travelled from the source to us.

$$\tau_\nu = -\int_0^s \alpha_\nu ds' = \int_s^0 \alpha_\nu ds'. \quad (\text{A.5})$$

The optical depth is thus integrated *against* the direction of travel with  $\tau_\nu=0$  at the observer and  $\tau_\nu = \infty$  at an infinite distance. It measures the photon-escape from a medium, and therefore describes the radiation as we see it.

The opacity can also be viewed upon as the inverse of the average distance travelled between collisions, or the *mean free path*,  $l$ , which is

$$l = \frac{vt}{n \sigma_\nu vt} = \frac{1}{n \sigma_\nu} = \frac{1}{\alpha_\nu}. \quad (\text{A.6})$$

The number of mean free paths, as measured along the ray's path is therefore another expression for the optical depth. If the extinction is high a photon will travel only a very short distance before it collides, and therefore it will be trapped within the medium. The radiation cannot escape the medium unless the optical depth is about one or less. Note, that the mean free path and the optical depth are different for photons of different frequencies.

The ratio of emission- and absorption coefficient is called the *source function*

$$S_\nu \equiv \frac{j_\nu}{\alpha_\nu}. \quad (\text{A.7})$$

The source function depends only on the local temperature of the cloud. The dimensions are the same as for the intensity, and these two quantities can be added or subtracted. The source function specifies the addition of photons along the path of the beam.

We can now rewrite Eq. (A.3) as

$$-\frac{dI_\nu}{\alpha_\nu ds} = I_\nu - \frac{j_\nu}{\alpha_\nu} \quad (\text{A.8})$$

$$\frac{dI_\nu}{d\tau_\nu} = I_\nu - S_\nu. \quad (\text{A.9})$$

### A.1.2 Solution of the transport equation

For pure extinction  $j_\nu = 0$ , and the transport equation will be reduced to

$$\frac{dI_\nu}{d\tau_\nu} = -I_\nu, \quad (\text{A.10})$$

which has the solution

$$I_\nu = I_{\nu,0} e^{-\tau_\nu}. \quad (\text{A.11})$$

The infalling intensity decreases exponentially by the optical depth along the ray.

The limit between small and large extinction is found at  $1/e$ , and  $\tau_\nu = 1$ . The gas is called *optically thick* if  $\tau_\nu > 1$  and *optically thin* if  $\tau_\nu < 1$ . An optically thin medium is one in which a photon can traverse the medium without being absorbed, whereas in an optically thick medium the photon will be absorbed.

In addition to extinction there is also emission

$$dI_\nu = j_\nu ds = S_\nu d\tau_\nu \quad (\text{A.12})$$

which must be added to the equation. This emission must be multiplied by a diminishing exponential to correct for the absorption from the emitting cloud.

With both these contributions the solution of the transport equation will be:

$$I_\nu(\tau_\nu) = I_{\nu,0} e^{-\tau_\nu} + \int_0^{\tau_\nu} S_\nu(\tau'_\nu) e^{-(\tau_\nu - \tau'_\nu)} d\tau'_\nu. \quad (\text{A.13})$$

If we assume that the cloud is homogeneous and the source function  $S_\nu$  is constant, the solution will be simple:

$$I_\nu(\tau_\nu) = I_{\nu,0} e^{-\tau_\nu} + S_\nu(1 - e^{-\tau_\nu}). \quad (\text{A.14})$$

Here, the first term represents the damping of the infalling intensity when the radiation passes through the cloud. The second term is the emission contribution from the cloud, corrected for absorption when it travels through the cloud. The resulting frequency dependent intensity is thus depending on the properties of the medium it travels through, such as the absorption coefficients and the density of the gas-particles, and also of the temperature.

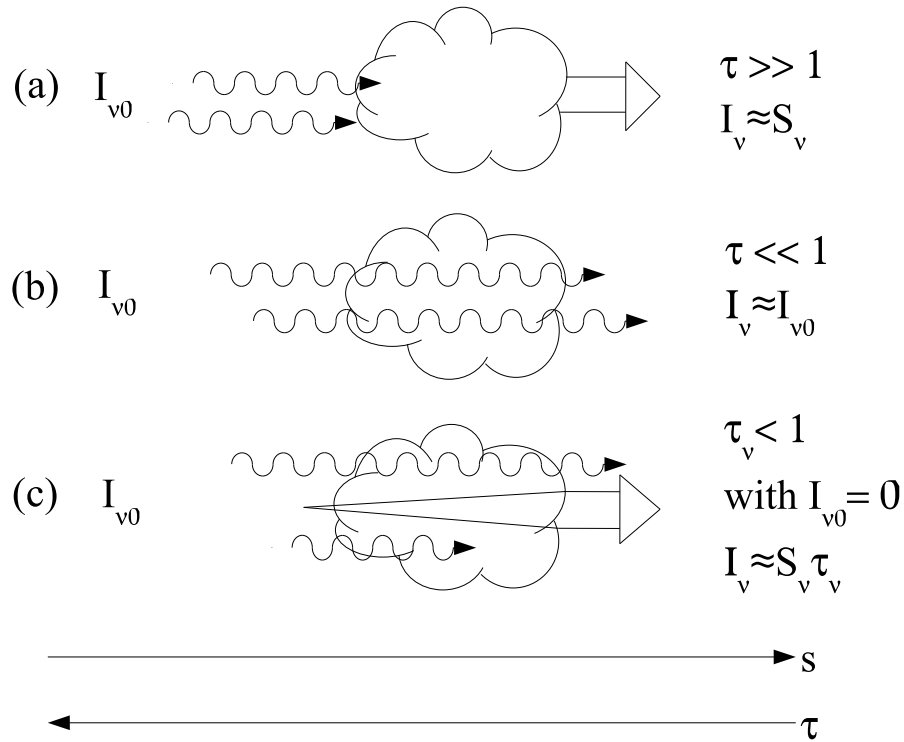


Figure A.1: Special cases in (a) the optically thick limit, (b) the extreme optically thin limit, and (c) the optically thin limit. Credit: Kaj Silander

### A.1.3 Special cases

There are three special cases which have ever more simple solutions than shown by Eq. (A.14), which occur in the optically thin and thick limits.

- Optically thick limit,  $|\tau| \gg 1$ .

If the gas is very dense and opaque then the optical depth will be very large and we will have

$$I_{\nu} \approx S_{\nu}. \quad (\text{A.15})$$

When we observe an optically thick medium we will obtain information about the emission from the surface of the cloud, as shown in Fig. A.1(a). The radiation can escape from the medium at a mean optical depth of approximately one and therefore an optically thick medium effectively blocks all infalling radiation as well as radiation from within the medium. The emergent intensity is only depending on the local temperature, and therefore observation of optically thick emission gives direct temperature information.

- Optically thin limit  $|\tau| < 1$ .

In the less extreme thin limit, but still with little intervening gas absorbing the intensity, the optical depth will be smaller than one. The exponential can then be expanded with a Taylor-series,  $e^{-\tau_\nu} \approx 1 - \tau_\nu$  and we will get:

$$I_\nu(\tau_\nu) \approx I_{\nu,0}(1 - \tau_\nu) + S_\nu \tau_\nu = I_{\nu,0} + (S_\nu - I_{\nu,0})\tau_\nu. \quad (\text{A.16})$$

This simplification is correct within 5% to 10% for an optical depth of 0.1 and 0.2, respectively. The source-function can very often vary substantially over a narrow frequency band, and this will give emission lines if the difference between  $S_\nu$  and  $I_{\nu,0}$  is positive, or absorption lines if its negative.

If there is no infalling radiation we will have

$$I_\nu \approx S_\nu \tau_\nu \quad (\text{A.17})$$

Observations of optically thin emission or absorption gives information about the total integrated emission along the line-of-sight as illustrated in Fig. A.1(c). Information about the density or column density (see Sect. A.3) can therefore be obtained.

- Optically extreme thin limit  $|\tau| \ll 1$ .

When the density of the intervening gas is very low and the optical depth is much below one, as seen from Eq. (A.17) the emergent intensity will simply be:

$$I_\nu(\tau_\nu) \approx I_{\nu,0} \quad (\text{A.18})$$

There is another special case that will not be treated any further in this work and that is when the optical depth is negative:

$$\tau_\nu \ll -1. \quad (\text{A.19})$$

As seen from Eq. (A.13), a negative optical depth will *increase* the intensity exponentially with  $\tau_\nu$ . In this case we have maser amplification.

### A.1.4 Discrete processes – spectral line theory

Atoms and molecules have discrete energy levels as described by quantum theory, which means that the radiation is quantised. There are various types of discrete energy levels, for example:

- *Electronic states of atoms and ions.* Transitions involving valence electrons have energies typically a few to hundreds of eV and the spectra are seen in visible or UV. When transitions involve inner shells the energies can be  $> \text{keV}$  and fall in the X-ray region.
- *Electronic states of molecules.* The energy is typically tenths to a few eV and the spectral region is infrared through the visible to the UV.
- *Vibrational states of molecules.* Molecules can also vibrate, and within the electronic states there are vibrational levels. The energy is typically a few tenths to one eV, and emitted in sub-mm or infrared.
- *Rotational states of molecules.* In addition to vibrational levels, the molecules can rotate at discrete energy levels. Within the vibrational levels there are rotational levels with very low energy differences. The emission of rotational lines are typically  $10^{-4} - 10^{-3}$  eV, and the spectra are therefore seen in the radio-regimes (mm and sub-mm). Fine- and hyperfine splittings of rotational states have even lower energies.

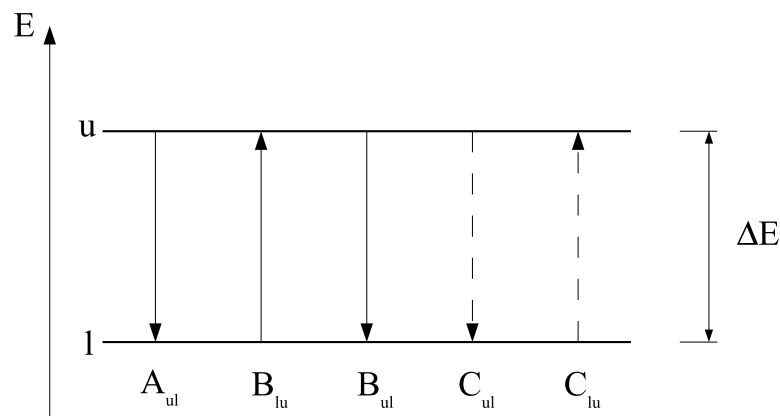


Figure A.2: A two-level system with transitions between the upper state  $u$  and the lower state  $l$ . The three radiative processes are described by the Einstein coefficients.

There are five processes for excitation or de-excitation between two states as illustrated in a two-level system in Fig. A.2. The energy difference between the states is  $\Delta E = h\nu$ . However, in any real system, there are many levels which may be connected by possible physical transitions.

The Einstein coefficients describe the probabilities for emission and absorption through the various processes. The Einstein A-coefficient is the transition probability for a *spontaneous de-excitation* per second per particle in the upper state  $u$  [ $s^{-1}$ ]. This is only depending on atomic or molecular parameters and not on the environment, and can be calculated as:

$$A_{ul} = \frac{16 \pi^3 \nu_{ul}^3 \mu^2 S_{ul}}{3 \epsilon_0 h c^3 g_u}, \quad (\text{A.20})$$

where  $\mu$  is the molecular dipole moment which is measured in laboratories, and  $g_u$  is the statistical weight of the upper level. This is the number of states with the same energy. For linear molecules  $g_u=2J+1$ , where  $J$  is the rotational quantum number.  $S_{ul}$  is the intrinsic line strength and the calculations depend on the symmetry of the molecule. The line strength and dipole moment can be found in different databases (see Sect. 4.3) or in the literature. The average lifetime in a state  $u$  is  $1/\sum_i A_{ul}$ , where the summation of  $A_{ul}$  is over all lower states  $l$ .

The next process is the *radiative excitation* which is described by the Einstein  $B_{lu}$  coefficient together with the frequency- and angle averaged intensity  $\bar{I}_{\nu_0}$ .  $B_{lu} \bar{I}_{\nu_0}$  describes the number of radiative excitations per second per particle in state  $l$ .

The Einstein coefficient for stimulated emission is the de-excitation per second per particle in state  $u$ , described by  $B_{ul} \bar{I}_{\nu_0}$ . The de-excitation is stimulated by a photon with the same energy as the difference between the upper and lower state, and the result is two photons with the same energy, in the same direction.  $B_{lu}$  and  $B_{ul}$  have dimensions of [ $W^{-1} m^2 Hz s$ ].

The last two processes are *collisional excitation* and *collisional de-excitation*. The  $C_{lu}$  and  $C_{ul}$  coefficients describes the number of collisional excitations, or de-excitations, per second per particle in state  $u$  or  $l$ , respectively [ $cm^{-3}s^{-1}$ ]. The coefficients depend on the velocities between the colliding particles, on the density, and on the nature of the interaction. Collision partners may be electrons, H,  $H_2$  or He, with  $H_2$  as the dominant collision agent in dense molecular clouds. As an example, a transition from state  $i$  to state  $j$  from a collision between an atom and an electron is described by:

$$n_i C_{ij} = n_i N_e \int_{v_0}^{\infty} \sigma_{ij}(v) f(v) v dv \quad (\text{A.21})$$

with  $n_i$  as the number density in state  $i$ ,  $N_e$  is the electron number density,  $\sigma_{ij}$  is the collisional cross section,  $f(v)$  is the velocity distribution, and  $v_0$  gives the threshold kinetic energy by  $1/2mv_0^2$ .

Generally, the Einstein coefficients are related to each other through

$$A_{ul} = \frac{2h\nu_{ul}^3}{c^2} B_{ul} \quad \text{and} \quad B_{ul} = \frac{g_l}{g_u} B_{lu} \quad (\text{A.22})$$

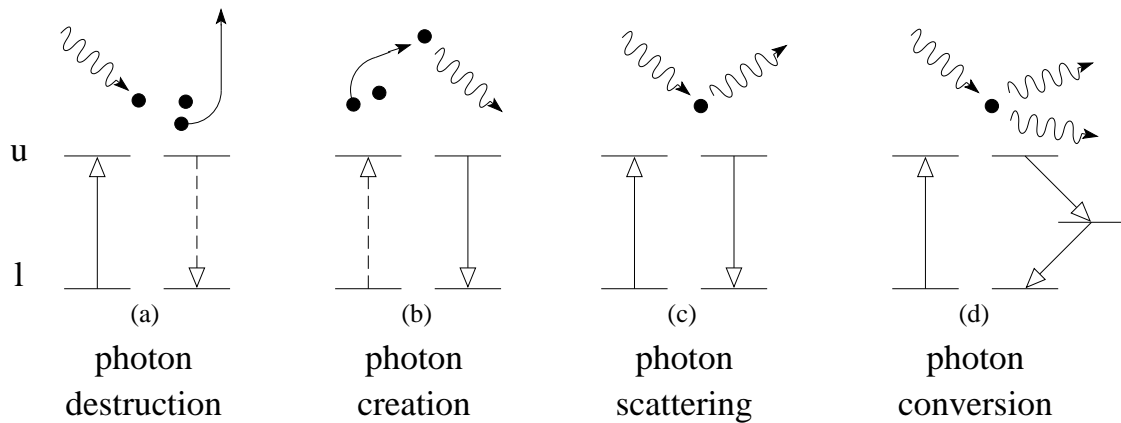


Figure A.3: An illustration of transitions between two states by different processes, which creates, destroys, scatter or converts photons. Credit: Kaj Silander

### A.1.5 Photon creation, destruction, scattering and conversion

- There are different kinds of interaction between discrete energy states. If a radiative excitation is followed by a collisional de-excitation, then a photon will be destroyed. Radiation will be transferred into kinetic energy of the gas which will *heat*. This is shown in Fig. A.3(a).
- If collisional excitation is followed by a radiative de-excitation (spontaneous or induced) a photon will be created, Fig. A.3(b). When this happens the kinetic energy in the colliding species will be transferred to radiation. By this process a gas is able to *cool* if the optical depth is low and the created photon is able to escape the cloud.
- When a radiative excitation is followed by radiative de-excitation the photon will change direction and the radiation will be re-distributed, Fig. A.3(c). In elastic scattering (resonant, Rayleigh or Thomson scattering) the frequency is maintained, while in inelastic scattering, such as Compton or inverse Compton scattering, the frequency will be altered. In the special case of stimulated emission, the direction is preserved.
- In the last shown process in Fig. A.3(d), a species is radiatively excited, and then followed by de-excitation in two (or several) steps. This will change the energies of an energetic photon into two or more photons with lower frequencies and thus with lower energies. By this the gas is able to *cool* if the cloud is optically thin for the created photons.

In the first two processes, the local kinetic energy of the gas particles and the radiation energy in the photons are transformed into one another. If these

processes are frequent, there will be strong coupling between the local radiation field and the local particle velocities, which is the same as the kinetic temperature of the gas. Thus, there will be equipartition of energy and thermodynamic equilibrium (TE) or Local TE applies (see Sect.A.1.6). However, if these processes are rare the temperatures of the radiation field and the gas may not be the same (Non-LTE case). In this case the photon might have been scattered several times after its creation. Thus, the radiation we see might not tell the observer anything about the conditions from where the photons are emitted.

### A.1.6 Types of equilibrium

- Thermodynamic Al equilibrium (TE).

This occurs in a very optically thick medium. For *every* subprocess detailed balance holds. This means that  $I_\nu = S_\nu = B_\nu$ , where  $B_\nu$  is the Planck function which describes the emission from a black-body

$$B_\nu = \frac{2h\nu^3}{c^2} \frac{1}{e^{h\nu/kT} - 1} \quad (\text{A.23})$$

where  $h$  is the Planck constant,  $c$  is the speed of light, and  $k$  is the Boltzmann constant. In TE the flux of emission is zero and no emission or absorption lines appear, only a thermal continuous emission as described by the Planck function.

The population of each level in TE is described by the *Boltzmann equation*, which is the number density in the upper state compared to that in the lower state. This also defines the *excitation temperature*  $T_{\text{ex}}$

$$\frac{n_u}{n_l} = \frac{g_u}{g_l} e^{-h\nu/kT_{\text{ex}}} \quad (\text{A.24})$$

where  $g_u$  and  $g_l$  are the statistical weights of the upper and lower states, and  $h\nu = E_u - E_l$ .

To compare the number density in state  $u$  with the total, we may write

$$\frac{n_u}{n_{\text{tot}}} = \frac{g_u}{Q(T)} e^{-h\nu/kT_{\text{ex}}} \quad (\text{A.25})$$

where  $Q(T)$  is the partition function and is the sum of all statistical weights,  $g_i$ , from all possible states:

$$Q(T) = \sum_{i=0}^{\infty} g_i e^{-E_i/kT_{\text{ex}}} \quad (\text{A.26})$$

The partition function depends on the excitation temperature but also on molecular constants and will therefore be different for different molecules.

The principle of detailed balance also holds for the collisions, which leads to a definition of the *kinetic temperature*  $T_K$

$$\frac{C_{lu}}{C_{ul}} \frac{n_u}{n_l} = \frac{g_u}{g_l} e^{-h\nu/kT_K} \quad (\text{A.27})$$

This relation holds generally, even outside TE.

When collisions dominate there will be strong coupling between the local radiation field and the local particle velocities. Thus, the temperature of the gas and radiation is in equilibrium and is the same, the gas is *thermalised* and  $T_{\text{rad}}=T_K=T_{\text{ex}}$ .

- Local thermodynamic equilibrium (LTE)

The mean free path of the particles is smaller than the scale of temperature variations, therefore the matter will experience a *local* TE and will be in equilibrium with the ambient kinetic temperature. However, the radiation temperature might deviate from the kinetic temperature and can vary slowly through the medium, but  $T_{\text{ex}} \approx T_K$ . Hence  $S_\nu = B_\nu$ , but  $I_\nu \neq B_\nu$ .

The Boltzmann equation still holds in LTE since the energy-distribution of matter is maintained locally by collisions and not by radiation.

- Statistic equilibrium (SE).

The assumption of statistical equilibrium implies that the radiation and the level populations are time independent and all upwards and downwards processes are balanced and

$$N_l (\bar{I}_{\nu_0} B_{lu} + n C_{lu}) = N_u (\bar{I}_{\nu_0} B_{ul} + n C_{ul} + A_{ul}), \quad (\text{A.28})$$

with  $\bar{I}_{\nu_0}$  as the frequency- and angle-averaged intensity,  $n$  as the number density of the collision partner, and  $N_l$  and  $N_u$  as the level populations in the lower and upper levels, respectively.

Since the temperatures are not the same, and might also differ between transitions in the same species, this calculation must be performed for every pair of states.

### A.1.7 Critical density

When the collisions in the gas start to dominate the downward transitions, in the two-level system the density is able to bring  $T_{\text{ex}}$  midway between  $T_{\text{rad}}$  and  $T_K$ . This density is referred to as the *critical density*. A commonly used first order approximation in a two level system is

$$n_{\text{crit}} = \frac{A_{ul}}{C_{ul}} \left( 1 + \frac{1}{e^{h\nu/kT} - 1} \right) \approx \frac{A_{ul}}{C_{ul}}. \quad (\text{A.29})$$

The approximation holds if  $h\nu \gg kT$  and is widely used as a first approximation of  $n_{\text{crit}}$ . A lower limit to the density in order to produce observable emission may be approximated by

$$n_{\text{min}} \gtrsim 10^{11} \frac{A_{\text{ul}} \sqrt{T_{\text{K}}}}{T_0} \text{ [cm}^{-3}\text{]} \quad (\text{A.30})$$

where we have used a mean velocity of the gas particles  $\langle v \rangle \approx 10^4 \sqrt{T_{\text{K}}} \text{ [cm s}^{-1}\text{]}$ , a cross-section approximated by the dimensions of a molecule,  $\sigma \sim 10^{-15} \text{ cm}^{-2}$ , and  $C_{\text{ul}} \approx n\sigma \langle v \rangle$ . This value must be multiplied with  $T_{\text{K}}/T_0$  for the excitation temperature to be at half the value of the kinetic temperature.

## A.2 Radioastronomy

In the radio spectral region the wavelengths are longer than in the visible and infrared light (from sub-mm to meter). This means that  $h\nu \ll kT$  and the exponent in the Planck function can be Taylor expanded to the *Rayleigh-Jeans law*

$$B_\nu(T) = \frac{2\nu^2}{c^2} kT. \quad (\text{A.31})$$

In radioastronomy also very often a *radiation temperature*  $J(T_{\text{ex}})$  is used, and is defined as

$$J(T_{\text{ex}}) = \frac{h\nu}{k} \frac{1}{e^{h\nu/kT_{\text{ex}}} - 1} \approx T_{\text{ex}}, \quad (\text{A.32})$$

where the approximation is valid only if  $h\nu \ll kT_{\text{ex}}$ . For temperatures  $T \approx 100\text{--}200 \text{ K}$ , and frequencies  $\sim 550 \text{ GHz}$ , the radiation temperature will differ from  $T_{\text{ex}}$  by approximately 10–15%. Accordingly,  $J(T_{\text{ex}})$  and not  $T_{\text{ex}}$  should be used in calculations.

The most important property of Rayleigh-Jeans law is the proportionality of the temperature and the radiation. This is so useful that the radiation from an extended source is measured by its *brightness temperature*,  $T_{\text{b}}$

$$T_{\text{b}} = \frac{c^2}{2k\nu^2} B_\nu. \quad (\text{A.33})$$

This is the temperature that would result in a given radiation if put into Rayleigh-Jeans law. Calibration procedures at radio telescopes, using thermal loads, allows  $J(T)$  to be expressed as  $T_{\text{b}}$ .

If this is applied to the equation of radiative transfer, Eq. (A.14), for an extended (i.e. the source fills the beam) isothermal medium we will get:

$$T_{\text{b}} = T_{\text{b}}(0) e^{-\tau_\nu} + T_{\text{ex}}(1 - e^{-\tau_\nu}). \quad (\text{A.34})$$

With no background radiation and for optically thin transition (A.34) simplifies to

$$T_b = T_{\text{ex}} \tau_\nu \quad (\text{A.35})$$

In case of an optically thick transition (A.34) simplifies to

$$T_b = T_{\text{ex}} \quad (\text{A.36})$$

### A.3 Column densities

Two properties of the gas are especially interesting: the temperature and column density which is defined as

$$N = \int_0^s n ds' \quad (\text{A.37})$$

in units of  $[\text{cm}^{-2}]$ . If we know the geometry of the source the density can then be calculated.

The column density can be obtained through different methods. With observations of a single line, either LTE is assumed and  $N$  can be calculated, or a statistical equilibrium model can be used. If a number of transitions are observed the rotation diagram method can be used, which is also described and used in Paper II. The resulting formula for the column density is found by expressing the absorption coefficient in terms of the Einstein coefficients

$$\kappa_\nu = \frac{h\nu}{4\pi} (n_l B_{lu} - n_u B_{ul}) \phi(\nu) \quad (\text{A.38})$$

where the normalised line profile  $\phi(\nu)$  is

$$\phi(\nu) = \frac{\sqrt{4 \ln 2}}{\Delta\nu \sqrt{\pi}} e^{-4 \ln 2 \left(\frac{\nu}{\Delta\nu}\right)^2}. \quad (\text{A.39})$$

The optical depth of a transition from an upper state,  $u$ , to a lower state,  $l$ , with the use of (A.25), (A.22) and (??) may be written as

$$d\tau_\nu = \kappa_\nu ds = \frac{h\nu_{ul}}{4\pi} (n_l B_{lu} - n_u B_{ul}) \phi_\nu ds \quad (\text{A.40})$$

$$= \frac{h\nu}{4\pi} \left( n_l \frac{g_u}{g_l} B_{ul} - n_u B_{ul} \right) \phi_\nu ds \quad (\text{A.41})$$

$$= \frac{h\nu}{4\pi} \left( \frac{n_u}{n_l} n_l e^{h\nu/kT_x} - n_u \right) \frac{c^2}{2h\nu^3} A_{ul} \phi_\nu ds \quad (\text{A.42})$$

$$= \frac{c^2}{8\pi\nu^2} A_{ul} n_u (e^{h\nu/kT_{ul}} - 1) \phi_\nu ds \quad (\text{A.43})$$

After integrating this along the line-of-sight we obtain

$$\tau_\nu = \frac{c^2}{8\pi k\nu_{ul}^2} A_{ul} N_u \left( e^{h\nu_{ul}/kT_{\text{ex}}} - 1 \right) \phi_\nu \quad (\text{A.44})$$

Integrating over an assumed Gaussian line profile, using the Boltzmann equation Eq. (A.25) for a relation between  $N_u$  and  $N_{\text{tot}}$ , and switching from frequencies to velocities (which is most common in radioastronomy) with the substitution  $d\nu = \nu/c dv$  we get

$$\tau_{\text{max}} = \sqrt{\frac{\ln 2}{16 \pi^3}} \frac{c^3}{\nu_{ul}^3 \Delta v} A_{ul} N_{\text{tot}} \frac{g_u}{Q(T)} e^{-E_u/kT_{\text{ex}}} (e^{h\nu_{ul}/kT_{\text{ex}}} - 1) \quad (\text{A.45})$$

With the assumption of optically thin emission, neglecting the background radiation, and assuming that the source fills the antenna main beam, the beam averaged upper state column density can be obtained from Eq. (A.44)

$$N_u = \frac{8\pi k\nu_{ul}^2}{hc^3} \frac{1}{A_{ul}} \int T_b dv \quad (\text{A.46})$$

The total column density of each species can then be found if we assume LTE, where all the excitation temperatures for all the energy levels are the same. The molecular population of each level is then given by the Boltzmann equation and the beam-averaged total column density becomes

$$N_{\text{tot}} = \frac{8\pi k\nu_{ul}^2}{hc^3} \frac{1}{A_{ul}} \frac{Q(T)}{g_u} e^{E_u/kT_{\text{ex}}} \int T_b dv \quad (\text{A.47})$$

assuming optically thin emission.

### A.3.1 Rotational diagram

If we want to calculate the total column density of a molecule we observe an optically thin transition, measure the integrated intensity and use it in (A.47). But the excitation temperature is still an unknown quantity. If we don't know it, we can make an educated guess and still be able to calculate the column density. A better way to establish the temperature is to use the rotational diagram method. If many transitions of the same species are observed, and LTE is assumed, which means that only one temperature characterises all the transitions, the excitation temperature can be calculated.

When we have observed a number of lines having a wide range of upper state energies, we can use the rotation diagram method. If we take the logarithm of the Boltzmann equation, Eq. (A.25), we obtain

$$\ln \frac{N_u}{g_u} = \ln \frac{N_{\text{tot}}}{Q(T)} - \frac{E_u}{kT_{\text{ex}}}. \quad (\text{A.48})$$

The left hand side in this equation is identical to the logarithm of Eq. (A.46) divided by the statistical weight  $g_u$ . We plot this quantity as a function of the upper state energy  $E_u$  in a semi-log plot. A least squares fit to the data will then produce a straight line with slope  $-1/T_{\text{rot}}$ . If we extrapolate the line to  $E_u = 0$  K, we obtain the total column density from the intersection of the y-axis,  $y_0$  and

$$N_{\text{tot}} = Q(T) e^{y_0}. \quad (\text{A.49})$$

The importance of a correctly calculated partition function is obvious.

However, the population distribution may not be characterised by a single rotational temperature. The temperature can vary due to density, excitation gradients along the line-of-sight, IR flux, sub-thermal excitation etc. This method also require optically thin transitions. The optical depth can change the slope of the rotation diagram and thereby affect both the rotation temperature and the column density. Once a transition has become optically thick, the value of  $N_u/g_u$  cannot increase any further. Then the derived total column density will be too low and need an optical depth correction factor (see Paper II).

# Bibliography

- [1] Abel, T., Bryan, G.L., Norman, M.L., 2002, *The Formation of the First Star in the Universe*, Science, vol 295, 93
- [2] Bennett, C.L., Fixsen, D.J., Hinshaw, G., Mather, J.C., Moseley, S.H., et al., 1994, *Morphology of the interstellar cooling lines detected by COBE*, ApJ, 434, 587
- [3] Bennett, C.L., Halpern, M., Hinshaw, G., Jarosik, N., Kogut, A., et al., 2003, *First-Year Wilkinson Microwave Anisotropy Probe (WMAP) Observations: Preliminary Maps and Basic Results*, ApJS, 148, 1
- [4] Blake, D.F., Jenniskens, P., *The Ice of Life*, Scientific American, Aug 2001, 37
- [5] Brack, A., 2002, *Water - the Spring of Life*, p 79 in *Astrobiology - the Quest for the Conditions of Life*, Horneck, G., & Baumstark-Khan, C., (Eds.), Springer Verlag
- [6] Cernicharo, J., and Crovisier, J., 2005, *Water in Space: The Water World of ISO*, SSRv, 119, 29
- [7] Cheung, A.C., Rank, D.M., Townes, C.H., Thornton, D.D., and Welch, W.J., 1968, *Detection of NH<sub>3</sub> molecules in the interstellar medium by their microwave emission*, Phys Rev Letters, 21, 1701
- [8] Cheung, A.C., Rank, D.M., Townes, C.H., Thornton, D.D., and Welch, W.J., 1969, *Detection of Water in Interstellar Regions by its Microwave Radiation*, Nature, vol 221, 626
- [9] Choudhury, T.R., and Ferrara, A., 2006, *Updating reionization scenarios after recent data*, MNRAS, 371, L55
- [10] de Bernardis, P., Dubrovich, V., Encrenaz, P., Maoli, R., Masi, S., et al., 1993, *Search for LiH lines at high redshift*, A&A, 269, 1
- [11] Doty, S.D., van Dishoeck, E.F., van der Tak, F.F.S., and Boonman, A.M.S., 2002, *Chemistry as a probe of the structures and evolution of massive star-forming regions*, A&A, 389, 446
- [12] Dubrovich, V., 1977 *Molecules of cosmological origin*, SvAL, 3, 128

- [13] Dubrovich, V., and Bajkova, A.T., 2003, *A Difference Method of Searching for Spectral-Spatial Fluctuations of the Cosmic Microwave Background Radiation* *AstL*, 29, 567L
- [14] Ehrenfreund, P. and Charnley, S.B., 2000, *Organic Molecules in the Interstellar Medium, comets, and meteorites*, *ARA&A*, 38, 427
- [15] Evans II, N.J., 1999, *Physical Conditions in Regions of Star Formation*, *ARA&A*, 37, 311
- [16] Genzel, R., and Stutzki, J., 1989, *The Orion Molecular Cloud and Star-forming region*, *ARA&A*, 27, 41
- [17] Gibb, E.L., Whittet, D.C.B., Boogert, A.C.A., and Tielens, A.G.G.M., 2004, *Interstellar Ice: The Infrared Space Observatory Legacy*, *ApJS*, 151, 35
- [18] Glover, S., 2005, *The formation of the first stars in the universe*, *SSRv*, 117, 445
- [19] Goldsmith, P.F., and Langer, W.D., 1978, *Molecular cooling and thermal balance of dense interstellar clouds*, *ApJ*, 222, 881
- [20] Hartquist, T.W., (Ed.), 1990, *Molecular Astrophysics*, Cambridge University Press
- [21] Hartquist, T.W., & Williams, D.A., 1995, *The chemically controlled cosmos*, Cambridge University Press
- [22] Hartquist, T.W., & Williams, D.A., 1998, *The molecular astrophysics of stars and galaxies*, Oxford University Press
- [23] Hasegawa, T.I., Kwok, S., Koning, N., Volk, K., Justtanont, K., et al., 2006 *Observations of the Circumstellar Water  $1_{10}-1_{01}$  and Ammonia  $1_0-0_0$  Lines in IRC +10216 by the Odin Satellite*, *ApJ*, 637, 791
- [24] Hashimoto, M., and Kamikawa, T., 2003, *Effects of a decaying cosmological term on the formation of molecules and first objects*, *ApJ*, 598, 13
- [25] Hjalmarson, Å., Bergman, P., Biver, N., Florn, H.-G., Frisk, U., et al. , 2005, *Recent astronomy highlights from the Odin satellite*, *AdSpR*, 36, 1031
- [26] Hollenbach, D.J., & Thronson, Jr., H.A., 1987, (Eds), *Interstellar Processes*, Reidel Publishing Company
- [27] Kaufmann, M.J., and Neufled, D.A., 1996, *Far-infrared water emission from magnetohydrodynamic shockwaves*, *ApJ*, 456, 611
- [28] Lepp, S., Stancil, P.C., and Dalgarno A., 2002, *Atomic and molecular processes in the early Universe*, *JPhB*, 35, 57

- [29] Levy, E.H., & Lunine, J.I., (Eds.), 1991, *Protostars and Planets III*, University of Arizona Press
- [30] Lis, D.C., Blake, G.A., and Herbst, E., (Eds.), 2005, *Astrochemistry: Recent Successes and Current Challenges*, Proc. IAU Symposium 231, Cambridge University Press
- [31] Liseau, R., and the O<sub>2</sub>din Team, 2005, *Odin Detection of O<sub>2</sub>*, IAU Symposium No. 231: Recent Successes and Current Challenges, Lis, D.C., Blake, G.A., and Herbst, E., (Eds.), 301
- [32] Longair, M.S., 1998, *Galaxy formation*, Springer Verlag
- [33] Lovas, F.J., 2003, *Spectral Line Atlas for Interstellar Molecules (SLAIM03) Ver.1*, private communication and CD
- [34] Mannings, V., Boss, A.P., Russell, S.S., (Eds.), 2000, *Protostars and Planets IV*, Tucson: University of Arizona Press
- [35] Maoli, R., Melchiorri, F., and Tosti, D., 1994, *Molecules in the postrecombination universe and microwave background anisotropies*, ApJ, 425, 372
- [36] Maoli, R., Ferrucci, V., Melchiorri, F., Signore M., and Tosti, D., 1996, *Molecular signals from primordial clouds at high redshift*, ApJ, 457, 1
- [37] Mather, J.C., Hauser, M.G., Bennett, C.L., Boggess, N.W., Cheng, E.S., et al., 1990, *Early results from the Cosmic Background Explorer*, LIACo, 29, 25
- [38] Melnick, G.J., Stauffer, J.R., Ashby, M.L.N., Bergin, E.A., Chin, G., et al., 2000, *The Submillimeter Wave Astronomy Satellite: Science Objectives and Instrument Description*, ApJ, 539, L77
- [39] Melnick, G.J., Bergin, E.A., 2005, *The legacy of SWAS: Water and molecular oxygen in the interstellar medium*, Adv. in Space Research, 36, 1027
- [40] Müller, H.S.P., Thorwirth, S., Roth, D.A., and Winnewisser, G., 2001, A&A, 370, L49
- [41] Neufeld, D.A., Lepp, S., and Melnick, G.J., 1995, *Thermal balance in dense molecular clouds: Radiative cooling rate and emission-line luminosities*, ApJ, 100, 132
- [42] Nilsson, J.S., Gustafsson, B., and Skagerstam, B.S., (Eds), 1991, *The birth and early evolution of Our Universe*, Proc. Nobel Symposium no. 79, Physica Scripta Vol T36
- [43] Nordh, H.L., von Schéele, F., Frisk, U., Ahola, K., Booth, R.S., et al., 2003, *The Odin orbital observatory*, A&A, 402, L21

- [44] O'Shea, B.W., and Norman, M.L., 2006, *Population III Star Formation in a  $\Lambda$ WDM Universe*, ApJ, 648, 31
- [45] Pagani, L., Olofsson, A.O.H., Bergman, P., Bernath, P., Black, J.H., et al, 2003, *Low upper limits on the O<sub>2</sub> abundance from the Odin satellite*, A&A, 402, L77
- [46] Pfalzner, S., Kramer, C., Staubmeier, C., and Heithausen, A., 2004, *The Dense Interstellar Medium in Galaxies*, Proc. 4th Cologne-Bonn-Zermath Symposium, Springer Verlag
- [47] Pickett, H.M., Poynter, R.L., Cohen, E.A., Delitsky, M.L., JPearson, J.C., and Muller, H.S.P., 1998, *Submillimeter, and Microwave Spectral Line Catalog*, J.Quant.Spectrosc. & Rad.Transfer, 60, 883
- [48] Rohlfs, K., & Wilson, T.L., (Eds.), 2004, *Tools of Radio Astronomy*, Springer Verlag
- [49] Rutten, R.J., 1991, *The Generation and Transport of Radiation*, 4th ed., compiled in March 1995 by Dan Kiselman
- [50] Rydbeck, O., Hjalmarson, Å., 1985, *Radio observations of Interstellar Molecules, of their behaviour, and of their physics*, in Diercksen et al. (Ed.): *Molecular Astrophysics*, Reidel Publishing company, p 45-175
- [51] Schöier, F.L., van der Tak, F.F.S., van Dishoeck E.F., and Black, J.H., 2005, *An atomic and molecular database for analysis of submillimetre line observation*, A&A, 432, 369
- [52] Shang, H.,; Allen, A., Li, Z-Y., Liu, C-F., Chou, M-Y., and Anderson, J., 2006, *A Unified Model for Bipolar Outflows from Young Stars*, ApJ, 649, 845
- [53] Spergel, D.N., Bean, R., Dore, O., Nolta, M.R., Bennett, C.L., et al., 2006, *Wilkinson Microwave Anisotropy Probe (WMAP) Three Year Results: Implications for Cosmology*, astro-ph/0603449
- [54] Tielens, A.G.G.M., *The Physics and Chemistry of the Interstellar Medium*, Cambridge University Press, 2005
- [55] van Dishoeck, E.F., Blake, G.A., Draine, B.T., and Lunine, J.I., 1993, *The chemical evolution of protostellar and protoplanetary matter*, in *Protostars and Planets III*, Levy, E.H., and Lunine, J.I., (Eds.), University of Arizona Press, 163
- [56] Wirström, E.S., Bergman, P., A.O.H. Olofsson, et al. , 2006, *Odin CO and <sup>13</sup>CO J = 5 – 4 mapping of Orion KL – a step towards accurate water abundances*, A&A, 453, 979

- [57] Zel'Dovich, Y.B., 1978, *Spectral lines of prestellar origin*, Pis'ma Astron. Zh., 4, 165